Solid-State ^{93}Nb and ^{13}C NMR Investigations of Half-Sandwich Niobium(I) and Niobium(V) Cyclopentadienyl Complexes

Andy Y. H. Lo,[†] Thomas E. Bitterwolf,[‡] Charles L. B. Macdonald,[†] and Robert W. Schurko*,[†]

Department of Chemistry and Biochemistry, University of Windsor, Windsor, Ontario, Canada N9B 3P4, and Department of Chemistry, University of Idaho, Moscow, Idaho 83844-2343

Received: April 25, 2005; In Final Form: June 7, 2005

Solid-state ^{93}Nb and ^{13}C NMR experiments, in combination with theoretical calculations of NMR tensors, and single-crystal and powder X-ray diffraction experiments, are applied for the comprehensive characterization of structure and dynamics in a series of organometallic niobium complexes. Half-sandwich niobium metallocenes of the forms Cp′Nb(I)(CO)$_4$ and CpNb(V)Cl$_4$ are investigated, where Cp = $C_5H_5^-$ and Cp′ = $C_5H_4R^-$ with R = COMe, CO_2Me, CO_2Et, and $COCH_2$Ph. Anisotropic quadrupolar and chemical shielding (CS) parameters are extracted from ^{93}Nb MAS and static NMR spectra for seven different complexes. It is demonstrated that ^{93}Nb NMR parameters are sensitive to changes in temperature and Cp′ ring substitution in the Cp′Nb(I)(CO)$_4$ complexes. There are dramatic differences in the ^{93}Nb quadrupolar coupling constants (C_Q) between the Nb(I) and Nb(V) complexes, with C_Q between 1.0 and 12.0 MHz for Cp′Nb(CO)$_4$ and C_Q = 54.5 MHz for CpNbCl$_4$. The quadrupolar Carr−Purcell Meiboom−Gill (QCPMG) pulse sequence is applied to rapidly acquire, in a piecewise fashion, a high signal-to-noise ultra-wide-line ^{93}Nb NMR spectrum of CpNbCl$_4$, which has a breadth of ca. 400 kHz. Solid-state ^{93}Nb and ^{13}C NMR spectra and powder XRD data are used to identify a new metallocene adduct coordinated at the axial position of the metal site by a THF molecule: CpNb(V)Cl$_4$·THF. ^{13}C MAS and CP/MAS NMR experiments are used to assess the purity of samples, as well as for measuring carbon CS tensors and the rare instance of one-bond ^{93}Nb, ^{13}C *J*-coupling, $^1J(^{93}\text{Nb},^{13}\text{C})$. Theoretically calculated CS and electric field gradient (EFG) tensors are utilized to determine relationships between tensor orientations, the principal components, and molecular structures.

Introduction

Since the discovery of ferrocene,[1,2] metallocenes have captured the imagination of many chemists, due to their assortment of fascinating structures, variation in coordination chemistries, and their prevalence in many technologically important materials and industrial processes.[3−9] Solid-state structures of the monomeric half-sandwich niobium metallocenes of the forms Cp′Nb(I)(CO)$_4$ and Cp′Nb(V)Cl$_4$, along with other metallocenes of this motif, have been of great interest over the last decade. Cp′ is generally an η^5-coordinated cyclopentadienyl ring that may be substituted by a variety of functional groups. The carbonyl niobocenes can be synthesized under high pressure from Cp′NbCl$_4$,[10,11] and can potentially serve as building blocks in photochemically reactive organometallic polymers.[12,13] They are also used to produce phosphine derivatives, which may exhibit catalytic behavior in homogeneous H- and CO-transfer reactions.[14] The Cp′Nb(CO)$_4$ complexes have been characterized with single-crystal X-ray diffraction,[10,11,15,16] IR spectroscopy,[10,11,14] gas-phase photoelectron spectroscopy,[17] microwave spectroscopy,[18] and ^{93}Nb solution NMR.[10,14,16,19] The chlorinated niobocenes have been used extensively in the syntheses of half-sandwich (imido)-niobium complexes;[20,21] however, in comparison to Nb(I) complexes, fewer structural characterizations have been reported. For instance, phosphine adducts of CpNbCl$_4$[22] and Cp*NbCl$_4$[23] (Cp* = $C_5Me_5^-$) have been structurally characterized by single-crystal X-ray diffraction, multinuclear solution NMR, IR, EPR, and mass spectroscopy (MS). In terms of solid-state NMR, attempts at structural characterization of this class of compounds include a preliminary report on the solid-state ^{93}Nb NMR spectroscopy of CpNb(CO)$_4$,[24] and ^{31}P NMR experiments on a series of phosphine derivatives of half-sandwich niobium metallocenes.[25,26]

Standard ^{13}C, ^{1}H, and ^{2}H solid-state NMR experiments have long been used for the characterization of structure and dynamics in organometallic complexes such as metallocenes and bis-arene complexes.[27−40] More recently, experiments focusing upon the metal nuclei at the "heart" of metallocenes have proven to be excellent assessors of molecular structure and symmetry, intramolecular dynamics, and sample purity. Recent work in our research group has focused upon metallocenes containing half-integer quadrupolar nuclei (i.e., nuclear spin I = $^3/_2$, $^5/_2$, $^7/_2$, $^9/_2$), including ^{9}Be, ^{11}B, ^{23}Na, ^{25}Mg, ^{27}Al, and ^{91}Zr.[35,36,38,40−42] In addition, a number of other research groups have reported solid-state NMR studies of metallocenes containing both spin-$^1/_2$ and half-integer quadrupolar nuclei.[43−50]

Niobium has only one NMR-active isotope, ^{93}Nb, which has I = $^9/_2$ and 100% natural abundance. However, its moderately sized nuclear quadrupole moment ($Q(^{93}\text{Nb})$ = -0.32×10^{-28} m^2)[51] often results in severe quadrupolar broadening of central-transition NMR powder patterns, which in some cases is prohibitive in terms of routine spectral acquisition and interpretation. Nonetheless, solid-state ^{93}Nb NMR has been used to study a variety of different systems, including inorganic niobium halides,[52] intercalated H-bronzes of NbVO$_5$,[53] niobium

* To whom correspondence should be addressed: Phone: (519) 253-3000, ext 3548. Fax: (519) 973-7098. E-mail: rschurko@uwindsor.ca. Web: http://www.uwindsor.ca/schurko.

[†] University of Windsor.

[‡] University of Idaho.

10.1021/jp0521499 CCC: $30.25
Published on Web 07/27/2005

SCHEME 1: Molecular Structures of Half-Sandwich Niobium Metallocenes[a]

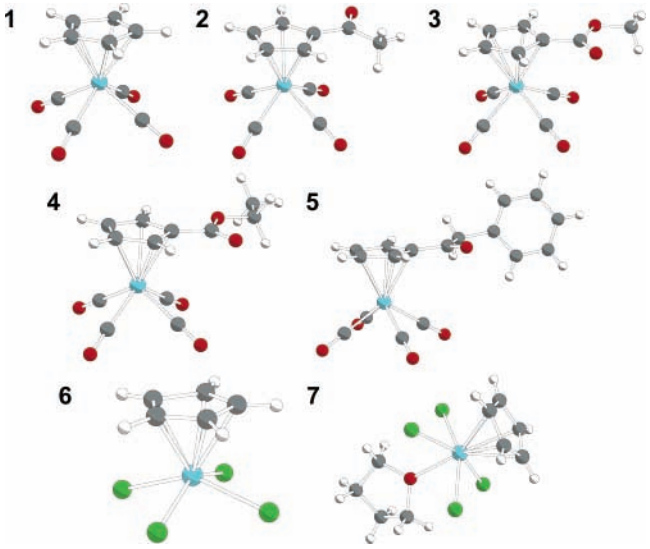

[a] Key: (**1**) (η^5-C_5H_5)Nb(CO)$_4$, (**2**) (η^5-MeOC-C_5H_4)Nb(CO)$_4$, (**3**) (η^5-MeO_2C-C_5H_4)Nb(CO)$_4$, (**4**) (η^5-EtO_2C-C_5H_4)Nb(CO)$_4$, (**5**) (η^5-$PhCH_2OC$-C_5H_4)Nb(CO)$_4$, (**6**) (η^5-C_5H_5)$NbCl_4$, and (**7**) (η^5-C_5H_5)$NbCl_4$·THF.

borides and deuterides,[54,55] and a variety of niobates.[56−70] There have also been a number of ^{93}Nb NMR studies featuring a variety of modern two-dimensional (2D) solid-state NMR experiments, including multiple quantum magic-angle spinning (MQMAS) and satellite-transition magic-angle spinning (STMAS) experiments, which are used for resolving peaks that may be obscured due to broad overlapping quadrupolar NMR patterns, as well as nutation and 2D-exchange NMR.[71−76]

Given the relatively favorable NMR characteristics of ^{93}Nb, solid-state ^{93}Nb NMR experiments on niobocene complexes could potentially act as fast, powerful probes of molecular structure, identity, and/or presence of solid-phase impurities, as well as lending insight into the fundamental origins of NMR interaction tensors in an important structural theme in organometallic chemistry. To these ends, we present a comprehensive solid-state ^{93}Nb and ^{13}C NMR study of niobium(I) carbonyl and niobium(V) chloride cyclopentadienyl complexes, including the parent compound, CpNb(CO)$_4$; complexes with singly substituted cyclopentadienyl rings, (η^5-C_5H_4R)Nb(CO)$_4$ (where R = COMe, CO_2Me, CO_2Et, and $COCH_2Ph$); and niobium(V) chlorides $CpNbCl_4$ and $CpNbCl_4$·THF (Scheme 1). For complexes which have extremely broad central-transition powder patterns, the quadrupolar Carr−Purcell Meiboom−Gill (QCPMG) pulse sequence[77] is applied to acquire sub-spectra in a piecewise manner, which are then co-added to produce the final ultra-wide-line ^{93}Nb NMR spectrum. The QCPMG pulse sequence has the potential to provide signal enhancement by an order of magnitude over standard spin−echo experiments, though its efficiency is limited by the T_2 relaxation time constant of the nucleus under study. QCPMG has also recently been coupled with MQMAS to produce spectra with high signal-to-noise ratio (S/N) and individually resolved sites.[78] Analytical and numerical simulations of magic-angle spinning (MAS) and static (i.e., stationary) ^{93}Nb NMR powder patterns are used to obtain the ^{93}Nb electric field gradient (EFG) and chemical shift (CS) tensor parameters. The ^{93}Nb NMR tensors are then correlated to molecular structure with the aid of theoretical calculations and/or X-ray data. Solid-state ^{13}C MAS and cross-polarization/MAS (CP/MAS) NMR experiments are used to determine carbon CS tensors for Cp′ ring carbons, to assess sample purity and identity, and to measure one-bond *J*-coupling between ^{13}C and ^{93}Nb.

Experimental Section

Materials. All Cp′Nb(CO)$_4$ compounds with Cp′ = C_5H_4R, where R = H (**1**), COMe (**2**), CO_2Me (**3**), CO_2Et (**4**), and $COCH_2Ph$ (**5**), were synthesized as previously described in the literature[10,15] and were used without further purification unless otherwise stated. CpNb(CO)$_4$ (**1**) was sublimed at 100 ± 10 °C prior to use (orange, needle-shaped crystals). $CpNbCl_4$ (**6**) was obtained from Aldrich, and $CpNbCl_4$·THF (**7**) was synthesized by the recrystallization of $CpNbCl_4$ in THF in a dry, nitrogen-filled glovebox. The THF was dried on a series of Grubb's type columns.[79] The $CpNbCl_4$/THF solution was stirred for 2 days to ensure all of the $CpNbCl_4$ solid dissolved into the solution. Solvent was then decanted and residual solvent was removed under vacuum for 2 h. Isolated crystals were needle-shaped with a pink/purple coloration.

Solid-State NMR. Solid-state ^{93}Nb and ^{13}C NMR experiments were conducted on a Varian Infinity Plus NMR spectrometer with an Oxford 9.4 T wide bore magnet operating at $\nu_0(^{93}Nb)$ = 97.6 MHz and $\nu_0(^{13}C)$ = 100.5 MHz, employing high-power proton decoupling ($\nu_1(^1H) \approx$ 35 to 110 kHz). Most of the NMR spectra were acquired with use of Varian/Chemagnetics 2.5 mm HX MAS and 4 mm HX MAS probes, while ^{93}Nb ultra-wide-line static NMR spectra of $CpNbCl_4$ were acquired with use of a 5 mm HX static probe. All samples were ground into fine powders under an inert atmosphere and tightly packed into zirconium oxide rotors, which were sealed with airtight Teflon caps.

Niobium chemical shifts were referenced to a 0.4 M $NbCl_5$ solution in dry CH_3CN with $\delta_{iso}(^{93}Nb) = 0.0$ ppm. A conventional Bloch decay sequence was employed for most MAS and static experiments. A Hahn-echo pulse sequence of the form $[(\pi/2)_x-\tau_1-(\pi)_y-\tau_2-acq]$ was employed to acquire a satellite-transition spectrum (SATRAS)[80] of **1**, static spectra of samples **2** and **5**, and both the MAS and static spectra of **7**, to avoid losing points in the beginning of the FIDs which may cause baseline distortions in the Fourier-transformed spectra. All Hahn-echo experiments acquired under conditions of MAS were rotor synchronized. For MAS experiments, samples were spun at 5 to 27 kHz, 330 to 370 000 transients were collected, and calibrated recycle times ranged from 0.2 to 1.0 s. The central-transition selective 90° pulse width ranged from 0.44 to 7.90 μs, corresponding to rf fields from 6.3 to 113.6 kHz. For static echo experiments, inter-pulse delays ranged from 60 to 75 μs, and between 220 and 21 000 transients were collected. For the static ^{93}Nb QCPMG experiments on **6**, selective 90° pulses were 0.84 μs ($\nu_1(^{93}Nb)$ = 59.5 kHz), inter-pulse delays were ca. 60 μs, calibrated recycle times were 0.5 s, and 30 MG loops were collected with 128 points per echo. Five sub-spectra were collected at 100 kHz transmitter offsets, with 4400 scans per spectrum. Variable-temperature (VT) static ^{93}Nb NMR experiments ranging from +100 to −140 °C were conducted on samples **1** and **7**, using parameters similar to those above (temperatures are accurate to within ±2 °C, based on previous calibrations). Additional static ^{93}Nb experiments were conducted on samples **1**, **3**, **5**, and **7** with a Bruker DRX 500 spectrometer ($\nu_0(^{93}Nb)$ = 122.2 MHz), equipped with a broad-band 5 mm HX probe. A selective 90° pulse width of 2.5 μs ($\nu_1(^{93}Nb)$ = 20.0 kHz) was used for **1** and **3**; while 36° (1.25 μs) and 30° (0.67 μs) pulses, corresponding to rf fields of 15.8 and 25 kHz, respectively, were used for **5** and **7**.

Carbon chemical shifts were referenced to TMS ($\delta_{iso}(^{13}C) = 0.0$ ppm) by setting the high-frequency resonance of solid adamantane to 38.57 ppm. Solid-state $^{13}C\{^1H\}$ MAS, CP/MAS, and variable-amplitude (VA) CP/MAS (in cases where fast spinning was utilized) NMR experiments were performed on all samples. The 90° pulse widths for ^{13}C MAS experiments ranged from 3.5 to 6.0 μs. Samples were spun between 1.95 and 14.0 kHz, the number of transients collected ranged from 420 to 3500, and calibrated recycle times ranged from 29 to 40 s. For ^{13}C CP/MAS NMR experiments, the ^1H 90° pulse widths were 1.9 to 3.5 μs, between 370 and 13 000 transients were collected, and recycle times varied from 5 to 20 s. Optimal contact times varied from sample to sample, ranging from 4 to 19 ms. During the contact time in VACP/MAS experiments, 10 or 15 steps of 4 to 19 ms length were applied, linearly ramping from 13.2 to 92.6 kHz on the ^{13}C channel. Several static ^{13}C CP experiments were attempted, but discontinued due to difficulties with orientation-dependent CP efficiencies. VT ^{13}C CP/MAS NMR experiments were conducted on **6**, with $\nu_{rot} = 1.9$ kHz and between 252 and 444 scans were collected.

Spectral Simulations. The EFG and CS parameters of all ^{93}Nb static and MAS spectra were obtained with analytical simulations using the WSOLIDS simulation package.[81] SIMPSON[82] was used to obtain numerical simulations of the ^{93}Nb SATRAS spectrum of **1** and the MAS NMR spectrum of **7**, and was run on a Dell Precision 420 workstation with dual 733 MHz pentium III processors running Red Hat Linux 6.2. The simulation was carried out by the *direct* method of powder averaging using the *zcw4180* crystal file, which is provided with the package. I_{1z} and I_{1p} were set as the start and detect operators, respectively. The number of γ angles was set to 100 and 30 for **1** and **7**, respectively.

Theoretical Calculations. Structural parameters of **1** through **5** used in the calculations were obtained from experimentally determined crystal structures,[10,11,15] with the exception of **4**, for which a structural geometry based on **3** was theoretically determined. The structure of **6** was constructed with geometry-optimized Cl positions, starting with a geometry based on **1**. The structure of **7** used in the calculations was obtained from a single-crystal X-ray diffraction experiment (vide infra). The Cp′ ring proton positions were optimized for all complexes at corresponding levels of theory.

Restricted Hartree−Fock (RHF) and hybrid density functional theory (B3LYP) calculations were carried out with use of the Gaussian 98 and 03 software packages[83,84] on a Dell Precision 420 workstation with dual 733 MHz Pentium III processors. Two different all-electron basis sets, 16s10p7d (4F) and 16s10p7d (6D),[85] were used for the Nb atoms, which correspond to valence shell electron configurations of $4d^35s^2$ and $4d^45s^1$, respectively. The 6-31G** and 6-311G** basis sets were used for all other atoms, while 6-311G(2d,p) and 6-311G(2df,p) basis sets, with and without diffuse functions, were applied in select calculations.

Calculations of NMR tensor parameters on the optimized gas-phase structures of **1** and **6** were also performed at select levels of theory. Embedded cluster molecular orbital (ECMO) calculations were also conducted on select species. In the ECMO calculations, a cluster (in this case, a neutral, isolated molecule) was embedded in a spherical lattice of point charges (e.g., with a radius of ca. 20 Å), which are determined from Mulliken population analyses or arbitrarily assigned.

The value of $C_Q(^{93}Nb)$ in Hz is obtained by multiplying the largest component of the EFG tensor (eq or V_{33}, expressed in au) by $(eQ/h) \times 9.7177 \times 10^{21}$ V m^{-2},[86] where $e = 1.602 \times 10^{-19}$ C, $Q(^{93}Nb) = -0.32 \times 10^{-28}$ m^2,[51] and h is Planck's constant. Niobium CS tensors were calculated by using the gauge-including atomic orbitals (GIAO) method.[87,88] The absolute shielding of the niobium nucleus is converted to the niobium chemical shift scale, using $NbCl_6^-$ ($\delta_{iso} = 0.0$ ppm) as the primary reference. The absolute shielding of the reference compound was obtained from a geometry-optimized $NbCl_6^-$ ion, using all levels of theory and all previously mentioned basis sets. Theoretical isotropic niobium chemical shifts can be obtained from $\delta_{iso} \approx \sigma_{ref} - \sigma_{sample}$.

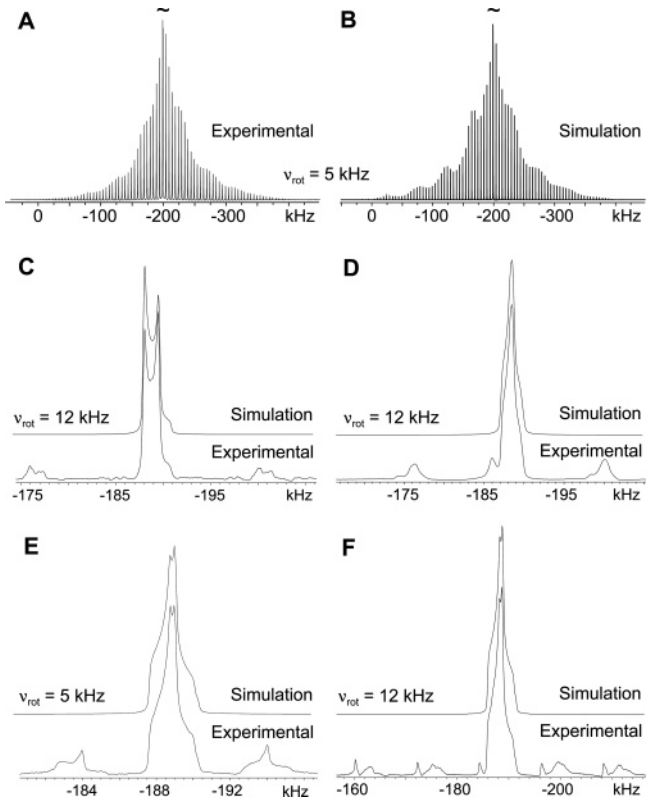

Figure 1. ^{93}Nb MAS NMR spectra of (A) **1** (experimental), (B) SIMPSON simulation of (A), and experimental and simulated ^{93}Nb MAS NMR spectra of (C) **2**, (D) **3**, (E) **4**, and (F) **5** acquired at 9.4 T.

X-ray Crystallography of $CpNbCl_4$·THF. The crystal used for the diffraction experiments was handled, selected, and coated in mineral oil prior to data collection. The data were collected on a Bruker Apex CCD diffractometer, using a graphite monochromator with Mo Kα radiation ($\lambda = 0.71073$ Å). A total of 1800 frames of data were collected with use of ω-scans employing a scan range of 0.3° and a counting time of 30 s per frame. The data were collected at −100 °C with a Kryoflex low-temperature device. Details of crystal data, data collection, and structure refinement are listed in the Supporting Information (Table S1). Data reduction was performed with SAINT.[89] The structure was solved by direct methods using SIR97[90] and refined by full-matrix least-squares on F^2 with anisotropic displacement parameters for most of the non-H atoms with SHELXL-97.[91] The cyclopentadienyl carbon was highly disordered and was modeled by using rings composed of isotropic carbon atoms in two different orientations; the relative occupancies of the orientations were refined to a ratio of 61:39. The corresponding carbon atoms in each ring were constrained to have identical temperature factors; however, no additional constraints were applied to the rings. All hydrogen atoms were placed in calculated positions (AFIX 23 for the methylene hydrogens and AFIX 43 for the aromatic hydrogens). The

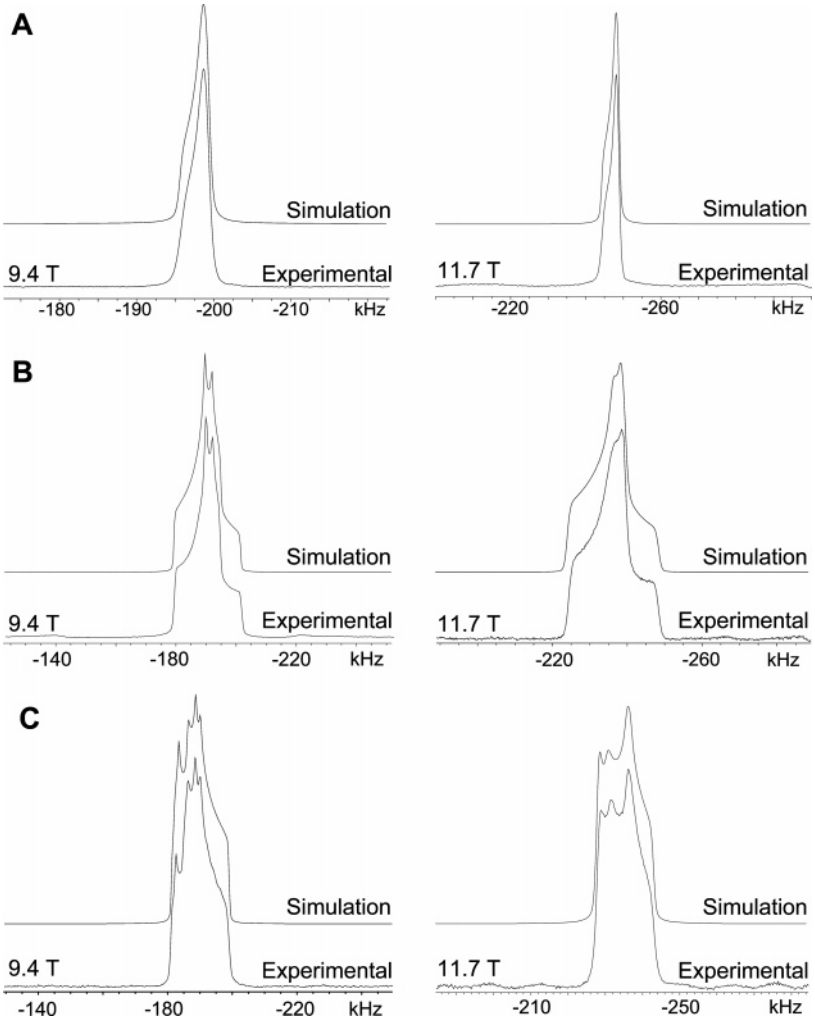

Figure 2. Experimental and analytically simulated ^{93}Nb static NMR spectra of (A) **1**, (B) **3**, and (C) **5** acquired at 9.4 and 11.7 T.

TABLE 1: Experimental ^{93}Nb NMR Parameters for Cp′NbX$_4$ Complexes

parameters	H, **1**[a]		COMe, **2**		CO_2Me, **3**		CO_2Et, **4**		$COCH_2$Ph, **5**		$CpNbCl_4$, **6**	$CpNbCl_4$·THF, **7**	
B_0 (T)	9.4	11.7	9.4	9.4	11.7	9.4	9.4	11.7	9.4	9.4	11.7		
C_Q[b] (MHz)	1.0(2)	1.2(2)	9.7(1)	9.0(3)	9.3(3)	8.7(4)	12.0(3)	12.3(3)	54.5(5)	38.4(4)	38.0(4)		
η_Q[b]	0.80(10)	0.70(10)	0.10(2)	0.79(4)	0.79(3)	0.89(9)	0.81(3)	0.84(3)	0.83(3)	0.17(7)	0.10(7)		
δ_{iso}[c] (ppm)	−2027(4)	−2023(4)	−1922(2)	−1924(4)	−1920(4)	−1920(1)	−1910(6)	−1904(6)	−600(30)	−703(12)	−715(12)		
Ω[c] (ppm)	35.0(5)	35.0(10)	125(3)	135(5)	140(5)	120(2)	91(4)	95(4)	150	320(10)	320(10)		
κ[c]	−0.90(5)	−0.90(5)	0.00(2)	0.10(5)	0.10(5)	0.20(4)	−0.4(2)	−0.2(2)	−0.6	−0.4(2)	−0.2(2)		
α[d]	90(20)	90(20)	70(5)	105(15)	120(15)	166(1)	36(7)	29(7)	90	155(2)	155(1)		
β	0(10)	0(10)	54(1)	44(3)	41(3)	63(1)	110(1)	109(1)	74	90(4)	86(4)		
γ	0(25)	0(30)	48(1)	62(23)	85(23)	34(1)	23(8)	31(8)	15	0(5)	0(1)		

[a] Singly substituted (η^5-C_5H_4R)Nb(CO)$_4$ complexes, with the substituents, R, being specified in the table for samples **1**−**5**. [b] The quadrupolar coupling constant and the quadrupolar asymmetry parameter of the ^{93}Nb EFG tensor are defined as $C_Q = eQV_{33}/h$ and $\eta_Q = (V_{11} - V_{22})/V_{33}$, respectively. [c] The isotropic value, span, and skew respectively of the niobium CS tensor, are defined as $\delta_{iso} = (\delta_{11} + \delta_{22} + \delta_{33})/3$, $\Omega = \delta_{11} - \delta_{33}$, and $\kappa = 3(\delta_{22} - \delta_{iso})/\Omega$. [d] α, β, and γ are the Euler angles between the ^{93}Nb EFG tensor and the niobium CS tensor in degrees.

function $\sum w(|F_o|^2 - |F_c|^2)^2$ was minimized, where $w = 1/[(\sigma(F_o))^2 + (0.0227P)^2 + (1.3514P)]$ and $P = (|F_o|^2 + 2|F_c|^2)/3$. No correction for secondary extinction effects was necessary. Neutral atom scattering factors and values used to calculate the linear absorption coefficient are from the International Tables for X-ray Crystallography (1992).[92] All figures were generated with SHELXTL.[93] Tables of positional, thermal, and metrical parameters are provided in the Supporting Information (Table S2). In addition, powder XRD experiments were conducted with a Bruker AXS D8 Discover powder X-ray diffractometer to assess the purity of bulk samples of **6** and **7**. Samples were loaded into 1.0 mm diameter capillary tubes and sealed under an inert atmosphere. Simulations of the powder XRD patterns from their corresponding known crystal structure were performed with PowderCell software.[94]

Results and Discussion

Solid-State ^{93}Nb NMR of Cp′Nb(CO)$_4$ Complexes. ^{93}Nb MAS NMR spectra of the parent compound, $CpNb(CO)_4$ (**1**), and singly substituted analogues (**2**−**5**) are shown in Figure 1, and corresponding static ^{93}Nb NMR spectra for compounds **1**, **3**, and **5** are displayed in Figure 2. Compound **1** possesses a very small quadrupolar interaction and does not display a second-order quadrupolar pattern in the MAS spectrum at 9.4 T. Simulations of the MAS spectrum of the complete spinning

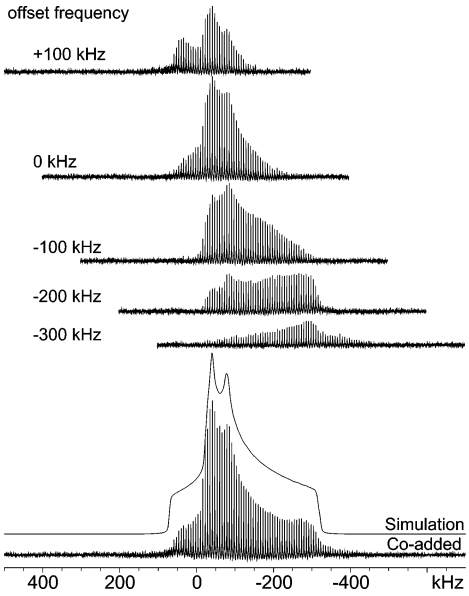

Figure 3. Piecewise static ^{93}Nb QCPMG NMR spectrum and analytical simulation of **6**, along with the transmitter offset frequencies of each sub-spectrum.

sideband manifold (Figure 1A), as well as a static powder pattern at two different magnetic field strengths (Figure 2A), were used to extract the values of $C_Q(^{93}Nb) = 1.0(2)$ MHz and $\eta_Q = 0.80(10)$ (Table 1). The value of $C_Q(^{93}Nb)$ is similar to that determined from gas-phase microwave experiments ($C_Q(^{93}Nb) = -1.8(6)$ MHz);[18] however, both C_Q and η_Q are in disagreement with a previous solid-state static ^{93}Nb NMR study on polycrystalline $CpNb(CO)_4$, where C_Q was determined to be 2.26 MHz and η_Q was assumed to be zero.[24] This discrepancy likely exists because, in this previous work, both the presence of niobium chemical shift anisotropy (CSA) and the fact that η_Q might be nonzero were not taken into account. To deconvolute the contributions from the second-order quadrupolar interaction and niobium CSA, two different magnetic fields are necessary.[95] Simulations of the complete MAS spinning sideband manifold (Figure 1B), as well as the static NMR spectra (Figure 2A), reveal a span of $\Omega = 35.0(5)$ ppm and $\kappa = -0.90(5)$. The niobium chemical shift, $\delta_{iso} = -2027(4)$ ppm, indicates one of the most shielded ^{93}Nb nuclei reported in the literature,[96] and is similar to values previously reported from solution NMR studies on $CpNb(CO)_4$, which range from ca. -2000 to -2050 ppm (different shift values are likely due to temperature and solvent effects).[10,14,16] The low chemical shift indicates a highly shielded niobium nucleus, which results from the Cp′−metal π-bonding interactions.[38,97] High magnetic shielding of niobium nuclei has also been observed in the ^{93}Nb NMR spectra of a variety of analogous systems.[14,19,98−100]

^{93}Nb MAS NMR spectra of compounds **2** through **5** are shown in Figure 1, parts C−F. All of the spectra display partially averaged second-order quadrupolar powder patterns and an array of spinning sidebands, indicating that the values of C_Q are large in comparison to those of **1**. The $C_Q(^{93}Nb)$ is observed to increase in the order **4** < **3** < **2** < **5** (Table 1); however, there is no general relationship between the nature of the substituents and the magnitude of C_Q (though C_Q in **5** is the largest in this series, possibly due to the bulkiness of the phenyl-containing substituent). The small value of C_Q in compound **1**, in comparison to those in compounds **2** through **5**, may arise from some sort of Cp′ ring motion in the former, which serves to dynamically reorient the ^{93}Nb EFG tensor (vide infra). The relatively large substituents on the Cp′ rings in the latter complexes would prevent such motional averaging, and correspondingly larger values of C_Q are observed. Interestingly, compounds **2** through **5** have higher isotropic chemical shifts than the parent compound, meaning that the niobium nuclei are slightly deshielded with respect to **1** due to substitution at the Cp′ ring. However, again there is no clear trend relating the nature or size of the substituents and the relative shift. Nevertheless, the combination of δ_{iso}, C_Q, and η_Q can be used to differentiate these chemically and structurally similar species. The rapidity with which these spectra can be acquired (i.e., 1 to 5 min) makes ^{93}Nb MAS NMR a useful "fingerprinting" tool for such compounds.

Static ^{93}Nb NMR spectra of compounds **3** and **5** acquired at 9.4 and 11.7 T are shown in Figure 2B,C. Compounds **3** and **5** have an increased niobium CSA with respect to **1** (see Table 1, and Figure S1 in Supporting Information for similar spectra of **2** and **4**). In compound **1**, the CS tensor is near axially symmetric (i.e., $\kappa = -0.90$, and δ_{11} is the pseudo-unique component); however, the presence of a substituent on the Cp ring results in nonaxial niobium CS tensors in all substituted complexes, attesting to the influence of substitution on the metal chemical shift tensor. In all cases, the ^{93}Nb EFG and CS tensors are not coincident. In fact, Euler angles obtained from simulations of the spectra indicate that relative orientations vary greatly between compounds (Table 1). The relationship between tensor orientation and molecular structure will be addressed in the discussion of theoretically calculated tensor orientations (vide infra).

Solid-State ^{93}Nb NMR and X-ray Diffraction of $CpNbCl_4$ and $CpNbCl_4$·THF. Static ^{93}Nb NMR spectra reveal that the magnitudes of $C_Q(^{93}Nb)$ in the niobium(V) half-sandwich complexes are very large compared to those in the niobium(I) complexes. In the case of $CpNbCl_4$ (**6**), the quadrupolar interaction is so large that the spectrum must be acquired in a piecewise fashion (Figure 3), since the entire breadth of the pattern cannot be uniformly excited with a single short pulse. Individual sub-spectra are acquired by using a short excitation pulse and 100 kHz offset frequencies. The offsets are chosen such that the sinc-like excitation profiles in the frequency domain, when co-added, form a rectangular excitation profile.[101] The final spectrum can be produced by either co-adding the sub-spectra[102,103] or skyline projection (see Figure S2).[104] Simulation of the powder pattern yields $\delta_{iso} = -600(30)$ ppm, $C_Q = 54.5(5)$ MHz, and $\eta_Q = 0.83(3)$. The replacement of the neutral CO ligands with negatively charged Cl ligands and the higher oxidation state of Nb result in a drastically different ^{93}Nb EFG tensor with an extremely augmented V_{33} component (as $C_Q = eQV_{33}/h$). The piecewise QCPMG spectra were only acquired at 9.4 T, so accurate extraction of CS tensor parameters is troublesome. Simulations reveal that a slightly better fit can be obtained with $\Omega = 150$ ppm and $\kappa = -0.6$ (Figure S2). Ab initio calculations presented later in the paper predict a larger Ω on the order of 450 ppm; this is clearly not the case, as a noticeable change in the breadth of the powder pattern and/or positions of the discontinuities would be apparent. The CSA makes a very small contribution to the quadrupolar-dominated pattern and the span likely has an upper limit near 300 ppm. Thus, it is difficult to extract the CSA in this case unless extremely high magnetic field strengths were to be applied.

The molecular structure of $CpNbCl_4$ has not been determined by X-ray diffraction methods, due to the difficulty in obtaining single crystals suitable for single-crystal X-ray diffraction experiments. To isolate a single crystal of $CpNbCl_4$, a recrystallization from dry THF was attempted (THF was found to have

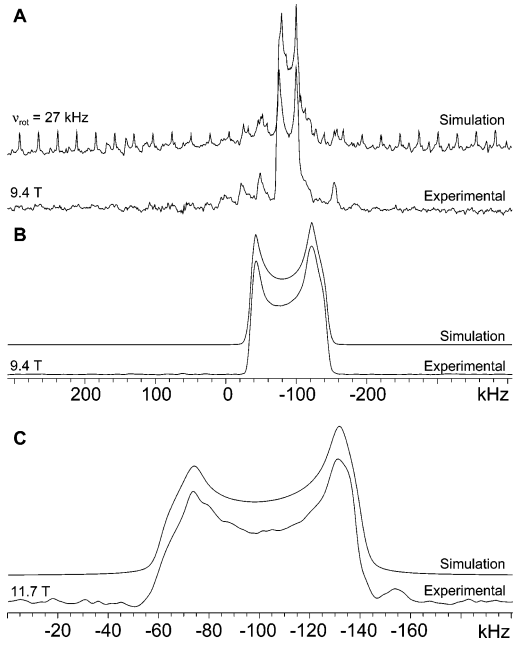

Figure 4. Experimental and simulated ^{93}Nb NMR spectra of **7**: (A) MAS and (B and C) static NMR powder patterns at two different magnetic field strengths. In part A, the numerical simulation includes excited central and satellite transitions, and assumes uniform excitation, accounting for the high intensities of the spinning sidebands in the simulated pattern.

the greatest solubility in comparison to MeCN, CH_2Cl_2, and toluene). The MAS and static ^{93}Nb NMR spectra of a fine powder of these crystals, along with numerical and analytical simulations, are shown in Figure 4. All of the NMR powder patterns and extracted parameters are very distinct from those of **6**, and the combination of ^{93}Nb NMR, ^{13}C NMR, and X-ray crystallographic data (vide infra) suggests that a single THF molecule coordinates from beneath the four Cl ligands (Scheme 1, $CpNbCl_4$·THF (**7**)). The THF ligand significantly alters the ^{93}Nb EFG and CS tensors. The quadrupolar parameters and isotropic chemical shift are obtained from fast-spinning MAS (ν_{rot} = 27 kHz) spectra as $\delta_{iso} = -703(12)$ ppm, $C_Q = 38.4(4)$ MHz, and $\eta_Q = 0.17(7)$. The breadth of the static pattern of **7** at 9.4 T is only 125 kHz, which is considerably less than the 450 kHz breadth of **6**; thus, the spectrum can be acquired in a single experiment at both 9.4 and 11.7 T. The value of $\eta_Q = 0.17$ in **7** implies that V_{33} is the pseudo-unique component of the EFG tensor, in contrast to the $\eta_Q = 0.83$ in **6**. In addition, the niobium nucleus is slightly more shielded due to a fairly dramatic change in the CS tensor. The span of the CS tensor is larger than those measured in all of the other complexes, though it is still nonaxial, with $\Omega = 320(10)$ ppm and $\kappa = -0.4(2)$.

Single-crystal X-ray diffraction experiments yielded a refined crystal structure which indicates that the $CpNbCl_4$ unit is directly coordinated at the niobium by a THF molecule (Figure 5). Powder X-ray patterns for **6** taken directly from the sample bottle and the recrystallized **7** are very different from one another (Figure 6, parts A and B, respectively). Simulation of the powder XRD pattern of **7** (Figure 6C) using the refined single-crystal structural data indicates that the molecular structure in the powdered microcrystalline sample is identical with that in the single-crystal phase. The structure of **7** is similar to those observed for phosphine and cyanide adducts of $CpNbCl_4$ and Cp^*NbCl_4 complexes.[22,23,105] Attempts to sublime **6** were unsuccessful at producing suitable single crystals for X-ray diffraction experiments; however, the combination of the NMR

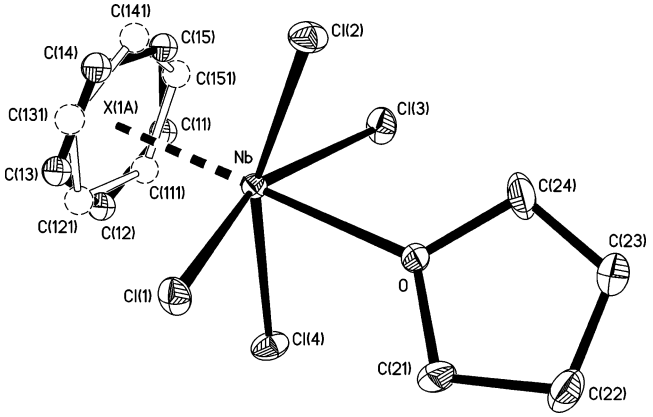

Figure 5. Thermal ellipsoid plot (30% probability surface) of the molecular structure of **7**. C11 to C15 (solid ellipsoids) represent the major occupancy atomic positions (61%) and C111 to C151 (dashed ellipsoids) the minor occupancy positions (39%). Note that X(1A) represents the centroid of the cyclopentadienyl ring with the highest occupancy. Hydrogen atoms are omitted for clarity.

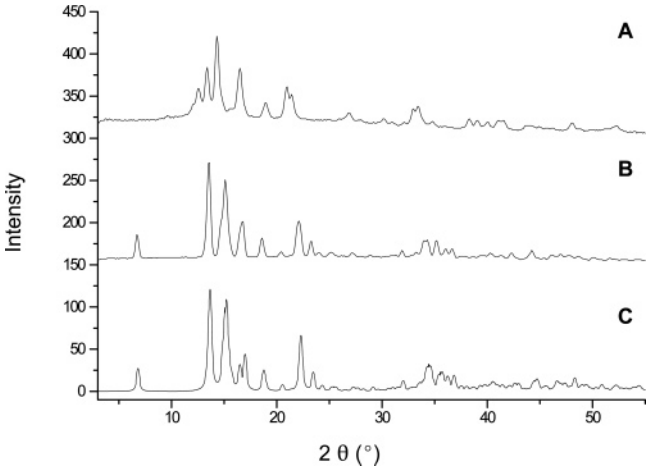

Figure 6. Experimental powder XRD patterns of (A) **6** and (B) **7** and (C) simulation of (B).

data and ab initio calculations presented below are used to propose potential solid-state structures for this system.

Solid-State ^{13}C NMR. Carbon-13 MAS and CP/MAS NMR spectra were acquired for all samples, and were utilized to measure carbon CS tensors, ^{13}C−^{93}Nb *J*-couplings, assess Cp ring dynamics, and ascertain the identity and purity of each sample. Carbon chemical shift assignments are summarized for all complexes in Table 2, and theoretically calculated carbon CS tensors of selected compounds are presented in Table 3.

The ^{13}C CP/MAS NMR spectra of complexes with unsubstituted Cp rings, $CpNb(CO)_4$ (**1**), $CpNbCl_4$ (**6**), and $CpNbCl_4$·THF (**7**), are shown in Figure 7, parts A, B, and C, respectively. Herzfeld−Berger analysis[106] of these spectra yields $\delta_{iso} = 96.6(1)$ ppm, $\Omega = 120(1)$ ppm, and $\kappa = 0.94(2)$ for **1**, which is quite distinct from that of **6** and **7**, with $\delta_{iso} = 131.4(1)$ ppm, $\Omega = 167(1)$ ppm, $\kappa = 0.65(1)$ and $\delta_{iso} = 130.4(1)$ ppm, $\Omega = 155(5)$ ppm, $\kappa = 0.7(1)$, respectively. The Ω and κ for **6** and **7** are quite unusual. For instance, Sayer[107] and Kentgens et al.[108] used solid-state ^{13}C NMR to study carbon CSA in some neutral and cationic half-sandwich Fe metallocenes, and measured carbon CS tensors with spans on the order of ca. 100 ppm and high axial symmetry ($\kappa \approx 1.0$). The much larger spans in **6** and **7** account for the higher isotropic chemical shifts, and result from decreased shielding in the plane of the Cp ring (i.e., increase in the chemical shifts of δ_{11} and δ_{22}). More interesting

TABLE 2: Structural Assignments of Experimental ^{13}C NMR Spectra for Cp′NbX$_4$ Complexes

H, **1**[a]	COMe, **2**	CO_2Me, **3**	CO_2Et, **4**	$COCH_2Ph$, **5**	$CpNbCl_4$, **6**	$CpNbCl_4$·THF, **7**
Cp, 96.6(1)	*C*H$_3$, 26.4(3) Cp(*C*$_\alpha$),[b] 94.1(1) and 104.3(1) Cp(*C*$_\beta$), 100.1(1) Cp(*C*$_{ipso}$), 110.0(3) Me-*C*O, 195.8(1)	*C*H$_3$, 53.3(2) Cp(*C*$_\beta$), 95.3(1) Cp(*C*$_\alpha$), 98.2(1) Cp(*C*$_{ipso}$), 100.3(3) Me-*C*O$_2$, 166.1(1) O*C*-Nb, 250(5)	*C*H$_3$, 16.0(2) *C*H$_2$, 60.6(2) Cp(*C*$_{\alpha,\beta}$), 99.1(1) Cp(*C*$_{ipso}$), 100.6(1) Et-*C*O$_2$, 165.5(2)	*C*H$_2$, 45.3(2) Cp(*C*$_{\alpha,\beta}$), 98.8(2) Cp(*C*$_{ipso}$), 111.7(3) Ph(*C*$_p$), 128.4(2) Ph(*C*$_o$), 129.5(2) Ph(*C*$_{ipso}$), 132.6(2) Ph(*C*$_m$), 134.6(2) O$_2$*C*-CH$_2$, 195.2(2) O*C*-Nb, 250.7(3)	Cp, 131.4(1)	THF(*C*$_\beta$), 26.8(3) THF(*C*$_\alpha$), 75.8(2) Cp, 130.4(1)

[a] Singly substituted (η^5-C$_5$H$_4$R)Nb(CO)$_4$ complexes, with the substituents, R, being specified in the table for samples **1**−**5**. [b] *C*$_\alpha$, *C*$_\beta$, and *C*$_{ipso}$ resonances of the Cp ring are well resolved only in the ^{13}C NMR spectrum of **2**.

TABLE 3: Carbon Chemical Shielding Tensor of the Cyclopentadienide Ligand in Unsubstituted CpNbX$_4$ Complexes

source	δ_{11}[a] (ppm)	δ_{22} (ppm)	δ_{33} (ppm)	δ_{avg}[b] (ppm)	δ_{iso}[c] (ppm)	Ω (ppm)	κ
$CpNb(CO)_4$, **1**	**137.8**[d]	**134.2**	**17.8**	**136**	**96.6(1)**	**120(1)**	**0.94(2)**
RHF/6-311G**	152.8	90.1	8.8	121.5	83.9	144	0.13
B3LYP/6-311G**	167.2	95.5	16.2	131.4	93	151	0.05
$CpNbCl_4$, **6**	**196.8**	**167.6**	**29.8**	**182.2**	**131.4(1)**	**167(1)**	**0.65(1)**
RHF/6-311G**	188.3	157.9	9.3	173.1	118.5	179	0.66
B3LYP/6-311G**	189.3	150.3	23.3	169.8	121	166	0.53
$CpNbCl_4$·THF, **7**	**189.8**	**166.6**	**34.8**	**178.2**	**130.4(1)**	**155(5)**	**0.7(1)**
RHF/6-311G**	177.8	162.2	4.8	170	114.9	173	0.82
B3LYP/6-311G**	179.9	160.6	18.9	170.3	119.8	161	0.76

[a] δ_{ii} are the principal components of the carbon CS tensor such that $\delta_{11} \geq \delta_{22} \geq \delta_{33}$. [b] Average value of δ_{11} and δ_{22}, with $\delta_{avg} = (\delta_{11} + \delta_{22})/2$. [c] Carbon CS tensor parameters: $\delta_{iso} = (\delta_{11} + \delta_{22} + \delta_{33})/3$, $\Omega = \delta_{11} - \delta_{33}$, and $\kappa = 3(\delta_{22} - \delta_{iso})/\Omega$. Carbon chemical shifts are referenced to TMS (experimental) or CO (theoretical), see Experimental Section for details. Averaged theoretical δ_{iso}, Ω, and κ are reported over the five distinct carbon sites of the Cp ring. [d] Experimental values are provided in boldface for comparison.

are the skews of the CS tensors. In **1**, the skew is near axially symmetric, resulting from time-averaging of the δ_{11} and δ_{22} components of the carbon CS tensor. This is indicative of unhindered rotation of the η^5-Cp rings, which normally occurs at temperatures greater than 77 K.[109] This is supported by theoretical calculations on **1**, which predict a nonaxially symmetric CS tensor; however, when the δ_{11} and δ_{22} components are averaged (representative of rapid, 5-fold reorientation of the Cp ring), there is very good agreement between experiment and theory. In **6** and **7**, the nonaxially symmetric skew might be a sign of hindered Cp ring rotation, which was previously observed by Gay et al. in VT ^{13}C NMR experiments on solid $CpMo(CO)_3R$, where R = Me, Et.[110] This assumption is also supported by the theoretical calculations, which predict CS tensor parameters in very good agreement with experimental values. The hindered rotation in **6** and **7** could be intramolecular and/or intermolecular in origin. Examination of the crystal structure of **7** reveals intermolecular contacts between the Cl ligands and the nearest H atom on the Cp ring (i.e., Cl···H ranging from 2.9 to 3.0 Å, Figure S3). Weak interactions of this kind were proposed by Blaurock et al. in the phosphine adducts of $CpNbCl_4$ complexes, in which almost identical Cl···H distances were observed (2.90 Å), resulting in polymeric ladders or dimers in the lattice.[23] Intermolecular interactions of this sort do not exist in the $CpNb(CO)_4$ molecule, accounting for the unhindered Cp rotation at temperatures above 77 K. Interestingly, our own VT ^{13}C CP/MAS experiments on **6** from +100 to −90 °C reveal no substantial changes in the carbon CSA (see Supporting Information, Figure S4), suggesting that unhindered Cp ring rotation may only occur near the decomposition temperature of $CpNbCl_4$ (which we have measured at ca. 130 to 140 °C).

In the ^{13}C CP/MAS NMR spectra of $CpNb(CO)_4$, a resonance corresponding to the carbonyl ligands is not observed, regardless of the length of the contact time. However, ^{13}C MAS NMR spectra acquired with a recycle time of 29 s reveal a very broad (spanning ca. 40 ppm), low intensity resonance centered at ca. 250 ppm (Figure 7A, inset). This resonance has a similar shift to that observed in the solution ^{13}C NMR spectrum of labeled $CpNb(*CO)_4$ (250 ppm), in which a ten peak multiplet is observed arising from $^1J(^{93}Nb,^{13}C) = 222$ Hz.[10]

Single substitution of the Cp ring breaks the 5-fold symmetry and results in a number of different Cp-ring carbon peaks. The substituted carbon is denoted as C_{ipso}, the neighboring carbons C_α, and the remaining carbons C_β. For instance, in the solid-state ^{13}C VACP/MAS NMR spectrum of **2**, the isotropic chemical shifts for C_{ipso}, C_β, and C_α are assigned as 110.0(3) ppm, 100.1(1) ppm, and 94.1(1) and 104.3(1) ppm, respectively (Figure 7D). There are two separate C_α peaks, since the rigid positioning of the side chain differentiates the electronic environments of these carbon sites. The assignments are made based upon both carbon chemical shielding parameters from ab initio calculations presented herein and analogous assignments made in the literature.[15] The wavy baseline arises from an overlap between the spinning sidebands, and the background signal from the Torlon-containing drive tip, and top and bottom spacers,[111] found exclusively in the 2.5 mm rotors used for **2**. In compounds **3** and **4** (Figure 7E,F), the various Cp carbon sites cannot easily be differentiated, due to either line broadening and/or the Cp ring ^{13}C nuclei having similar magnetic environments.

As in the case of **1**, NMR powder patterns corresponding to the carbonyl groups are either not observed or very weak and broad for **2**, **3**, and **4**. Interestingly, in the ^{13}C MAS NMR spectrum of **5** (Figure 8), which was acquired with a recycle time of 40 s, a very intense multiplet is observed that corresponds to the niobium-bound carbonyl groups. The ^{13}C multiplet has ten peaks, which result from indirect spin−spin coupling (*J*-coupling) with the ^{93}Nb nucleus (^{93}Nb is spin $^9/_2$ and 100% naturally abundant). The asymmetric appearance of the multiplet is the result of residual dipolar coupling[112] between ^{13}C and ^{93}Nb, which causes differential peak spacing and

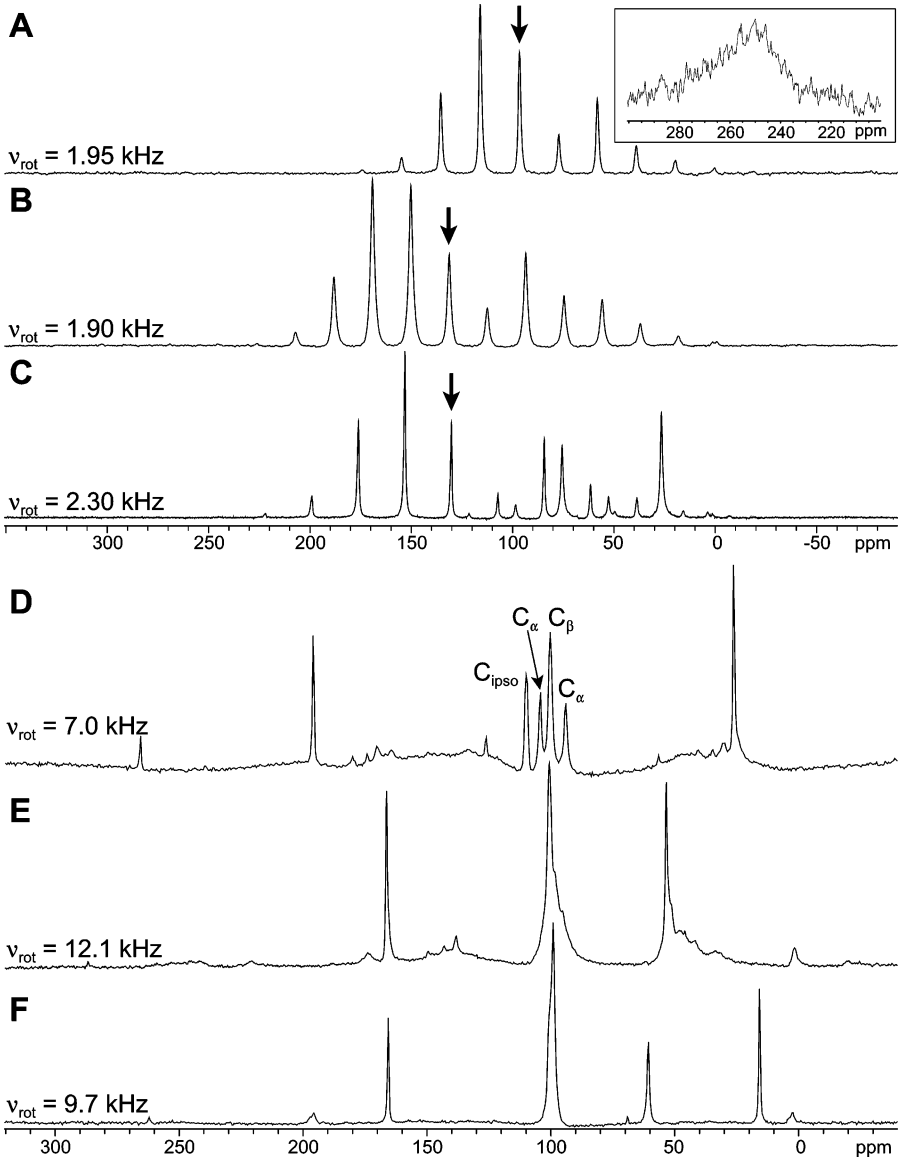

Figure 7. ^{13}C VACP/MAS NMR spectra for (A) **1**, (B) **6**, (C) **7**, (D) **2**, (E) **3**, and (F) **4** at 9.4 T. Arrows indicate isotropic resonances. Inset: The extremely low intensity of the O*C*-Nb resonance in the ^{13}C MAS NMR spectrum of **1** is presented.

broadening within the multiplet. The value of $^1J(^{93}\text{Nb},^{13}\text{C})$ is measured from the separation between the central peaks of the multiplet to be 220(1) Hz, which is very similar to that observed for labeled $\text{CpNb}(^{13}\text{CO})_4$.[10] It is often very difficult to observe such *J*-couplings between spin-$^1/_2$ and quadrupolar nuclei in solution and solid-state NMR experiments, due to rapid relaxation at the quadrupolar nucleus and scalar relaxation of the second kind at the spin-$^1/_2$ nucleus. There are a few other reported cases of similar couplings between spin-$^1/_2$ and spin-$^9/_2$ nuclei in the solid state, including $^1J(^{93}\text{Nb},^{31}\text{P})$ in a series of phosphine-containing half-sandwich niobium complexes,[25,26] $^1J(^{115}\text{In},^{31}\text{P})$ in the ^{31}P NMR spectra of a 1:1 adduct of indium tribromide and a triarylphosphine,[113] and $^2J(^{93}\text{Nb},^{29}\text{Si})$ in a niobium silicate ($Rb_4(NbO)_2(Si_8O_{21})$).[114] To the best of our knowledge, there has not been any report of $^1J(^{93}\text{Nb},^{13}\text{C})$ measured in solid-state ^{13}C NMR experiments.

Niobium NMR Interaction Tensors. In this section, we will first discuss the ^{93}Nb EFG tensors for the Nb(I) complexes, followed by the Nb(V) complexes, and then move on to a brief discussion of theoretical niobium chemical shielding tensors. We also present VT ^{93}Nb NMR spectra of complexes **1** and **7**, in an effort to make a prefatory examination on the effects of intramolecular motion on ^{93}Nb EFG tensor orientation. The theoretically calculated ^{93}Nb EFG and CS tensor parameters are presented in Tables 4−7, along with the corresponding experimental values for comparison. Due to the large number of calculations, only the most relevant data are presented within the paper (additional results are summarized in the Supporting Information, Tables S3−S7).

^{93}Nb EFG Tensors. The theoretical values of $C_Q(^{93}\text{Nb})$ are overestimated for **1** by more than an order of magnitude at all levels of theory. It is unlikely that the discrepancy between experiment and theory arises from insufficiently large basis sets or low levels of theory, since there are reasonable agreements between experiment and theory for compounds **2** through **5**, which are larger molecules, and where the substituted Cp rings do not rotate freely (Table 4). The experimental $\eta_Q = 0.8$ implies that V_{33} is not directed along the pseudo-rotational axis of the molecule (i.e., the molecular axis), and that V_{11} is the pseudo-unique component. Calculated ^{93}Nb EFG tensor orientations support this hypothesis, with V_{11} oriented nearly perpendicular to the central mirror plane, and V_{22} and V_{33} contained within the mirror plane, approximately along the direction of the Nb−CO bonds (e.g., $\angle(V_{22}-\text{Nb}-\text{Cp}_{cen}) = 42°$ and $\angle(V_{33}-\text{Nb}-$

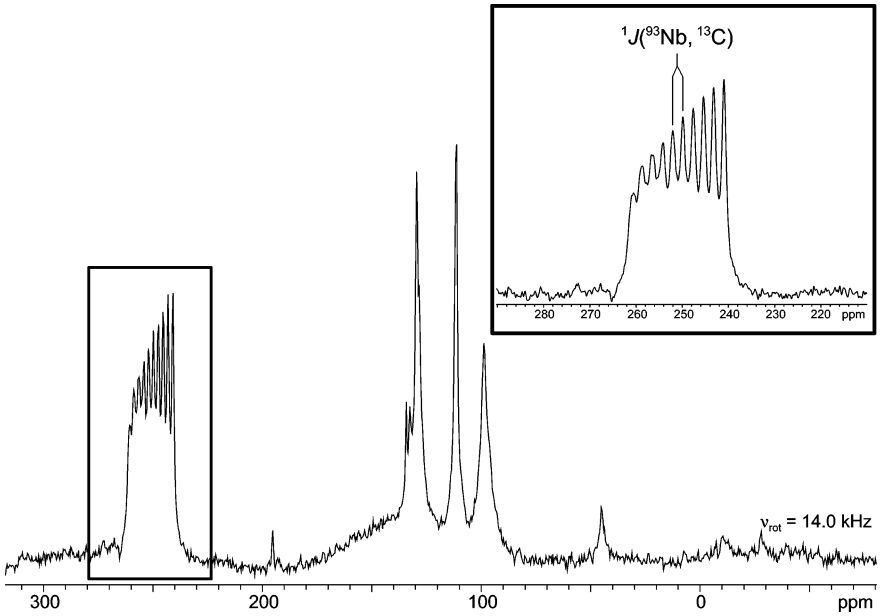

Figure 8. ^{13}C MAS NMR spectrum of **5** at 9.4 T. Inset: Expansion of the O*C*-Nb resonance showing the $^1J(^{93}Nb,^{13}C)$ pattern.

TABLE 4: Theoretical ^{93}Nb EFG Tensor Parameters in Nb(I) Complexes

source[a]	V_{11}[b] (au)	V_{22} (au)	V_{33} (au)	$\lvert C_Q\rvert$[c] (MHz)	η_Q
$CpNb(CO)_4$, **1**				**1.0(2)**[d]	**0.80(10)**
RHF/4F/6-311G**	−0.1334	−0.1821	0.3155	23.7	0.15
RHF/6D/6-311G**	−0.1083	−0.1892	0.2974	22.4	0.27
B3LYP/4F/6-311G**	−0.1172	−0.1565	0.2737	20.6	0.14
B3LYP/6D/6-311G**	−0.0941	−0.1715	0.2655	20	0.29
$(MeOC)CpNb(CO)_4$, **2**				**9.7(1)**	**0.10(2)**
RHF/4F/6-311G**	−0.0083	−0.0889	0.0973	7.3	0.83
RHF/6D/6-31G**	−0.085	−0.115	0.1999	15	0.15
RHF/6D/6-311G**	−0.0139	−0.0861	0.1	7.5	0.72
B3LYP/4F/6-311G**	0.0137	0.1067	−0.1204	9.1	0.77
B3LYP/6D/6-311G**	0.0027	0.116	−0.1187	8.9	0.95
$(MeO_2C)CpNb(CO)_4$, **3**				**9.0(3)**	**0.79(4)**
RHF/4F/6-311G**	−0.0187	−0.0885	0.1072	8.1	0.65
RHF/6D/6-311G**	−0.0067	−0.1188	0.1255	9.4	0.89
B3LYP/4F/6-311G**	−0.0119	−0.0714	0.0833	6.3	0.71
B3LYP/6D/6-311G**	0.0228	0.0952	−0.118	8.9	0.61
$(EtO_2C)CpNb(CO)_4$, **4**				**8.7(4)**	**0.89(9)**
RHF/4F/6-311G**	−0.0169	−0.0897	0.1066	8	0.68
RHF/6D/6-311G**	−0.0058	−0.1174	0.1232	9.3	0.91
B3LYP/4F/6-311G**	−0.0259	−0.0681	0.094	7	0.45
B3LYP/6D/6-311G**	0.0151	0.0992	−0.1143	8.6	0.74
$(PhH_2COC)CpNb(CO)_4$, **5**				**12.0(3)**	**0.81(3)**
RHF/4F/6-311G**	0.0154	0.1589	−0.1742	13.1	0.82
RHF/6D/6-311G**	0.0196	0.1533	−0.1729	13	0.77
B3LYP/4F/6-311G**	0.0551	0.1768	−0.2319	17.4	0.52
B3LYP/6D/6-311G**	0.0493	0.1774	−0.2267	17.1	0.57

[a] Source from theoretical work is in the form method/basis set (Nb)/basis set (all other atoms). [b] V_{ii} are the principal components of the ^{93}Nb EFG tensor such that $|V_{33}| \geq |V_{22}| \geq |V_{11}|$. [c] Absolute value of C_Q, where $C_Q = eQV_{33}/h$ and $\eta_Q = (V_{11} - V_{22})/V_{33}$. Theoretical C_Q are converted from atomic units to Hz (see Experimental Section for details). [d] Experimental values are provided in boldface for comparison.

$Cp_{cen}) = 48°$ according to RHF/6-311G** calculations, Figure 9A). However, the theoretical values of η_Q lie closer to the case of axial symmetry where $|V_{11}| \approx |V_{22}| < |V_{33}|$, in disagreement with experiment. This is puzzling, given that V_{22} and V_{33} appear to be oriented in very similar chemical environments.

It is very probable that the experimentally measured C_Q is the result of time averaging of the EFG tensor orientation resulting from some sort of intramolecular motion (i.e., the measured C_Q results from a time average of different orientations of V_{33}, perhaps from Cp ring rotation). Theoretical calculations of the SCF energy as a function of Cp ring rotation on both solid-state and gas-phase structures reveal 4-fold rotational barriers on the order of 12−14 and 5.5 kJ mol^{-1}, respectively (Figure 9B,C). Given the relatively low rotational barriers of Cp rings predicted by theory, it is likely that VT experiments conducted below 77 K could slow this intramolecular motion enough to observe the completely unaveraged EFG tensor components.[109] VT static ^{93}Nb NMR experiments conducted from +100 to −140 °C (Figure 10) partially support this hypothesis, revealing that C_Q increases as the temperature is decreased and η_Q changes from 1.0 (i.e., $V_{22} = V_{33}$) at high temperatures to 0.56 at the lowest temperature, meaning the tensor components are at least partially distinguished. These results suggest that higher temperatures result in averaging of

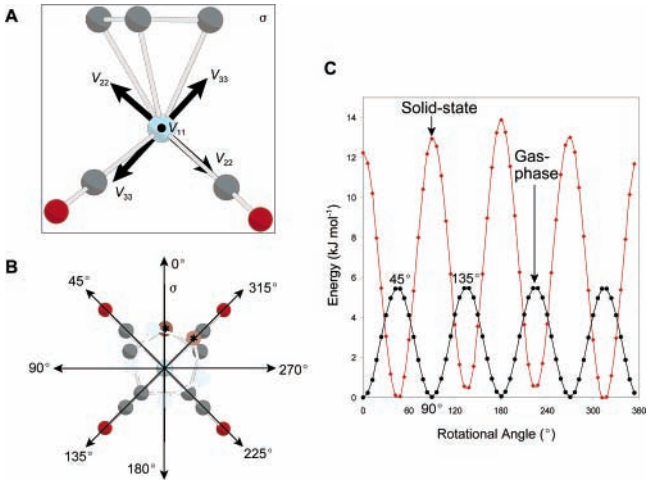

Figure 9. (A) ^{93}Nb EFG tensor orientation with respect to the molecular mirror plane (σ) and (B) schematic picture of the 5-fold rotation of the Cp ring about the molecular axis in **1**. In (B), 0° rotation is defined such that the mirror plane contains the unique Cp carbon (marked with an asterisk). (C) A plot correlates the SCF energy with the Cp ring rotation, defined in part B, for **1**.

the V_{22} and V_{33} components, while at lower temperatures, reduced motion results in their differentiation. Theoretical calculations also demonstrate that the magnitude and sign of C_Q, the value of η_Q, and the EFG tensor orientation all change as the orientation of the Cp ring is altered; however, a detailed experimental and theoretical study of this temperature-dependent EFG variation in **1** is beyond the scope of this paper (preliminary results are shown in the Supporting Information, Table S3).

Calculations on **2** using the 6-311G** basis set are relatively close to the experimental value of C_Q; however, in all cases, η_Q is predicted to be in the 0.7 to 1.0 range, in disagreement with experiment. The experimental value of $\eta_Q = 0.10(2)$ is anomalous in this series of Nb(I) complexes, implying that V_{11} and V_{22} are similar, and that V_{33} is oriented in a distinct electronic environment. Higher level calculations using 6-311G(2d,p) and 6-311G(2df,p) basis sets, with and without diffuse functions, did not result in improved agreement with experiment (see Supporting Information, Table S4). Interestingly, lower level RHF/6-31G** calculations overestimate C_Q considerably, but predict that $\eta_Q = 0.15$. From this particular calculation, the V_{33} component is oriented approximately toward the Cp ring ($\angle(V_{33}-\text{Nb}-\text{Cp}_{cen}) = 17.4°$), and the V_{22} points approximately in the direction of the side chain of the Cp ring (Figure 11A). The reason for the atypical EFG tensor in **2** compared to the others in this series of complexes is unknown at this time. On a side note of consequence, embedded cluster molecular orbital (ECMO) calculations do not alter the values of C_Q and η_Q significantly for **1**, **2**, or any of the other complexes discussed herein, suggesting that EFGs of intramolecular origin are dominant, and that major discrepancies between theory and experiment do not arise from intermolecular effects.

Calculations on complexes **3**, **4**, and **5** are in reasonable agreement with theory; notably, the RHF calculations of C_Q and η_Q are in good agreement with experimental values. The ^{93}Nb EFG tensors for **3** and **4** have similar orientations predicted at all levels of theory: V_{33} is oriented ca. 10° from an Nb−CO bond and V_{22} is in a similar environment. V_{11}, the pseudo-distinct component, is directed away from the Nb−CO bonds and the Cp ring (Figure 11B,C). Calculations predict that C_Q is smaller in all substituted complexes in comparison to the parent complex; this could in part be due to the Nb−Cp_{cen} distance, which is 2.090(2) Å for all substituted complexes, and 2.069(2) Å for the parent. In comparing **3** and **4** with **5**, the larger C_Q in the latter undoubtedly results from the decreased ground-state electronic symmetry resulting from substitution with the voluminous COCH_2Ph group. However, the EFG orientation in **5** is very similar to that encountered in the former complexes (Figure 11D).

All calculations on the Nb(V) complexes, **6** and **7**, predict a large increase in C_Q relative to the Nb(I) complexes, though there are some difficulties in obtaining quantitative agreement with experiment in both cases (Table 5). Since a crystal structure is not available for **6**, the solid-state structure had to be approximated from analogous crystal structures (details in the Experimental Section). Calculations on a geometry-optimized gas-phase CpNbCl_4 molecule consistently result in an overestimation of C_Q and near-zero η_Q, in disagreement with experiment (see the Supporting Information, Table S5). Approximating the structure of **6** by simply using the CpNbCl_4 framework from **7** without the THF ligand results in a severe overestimation of C_Q (as high as ca. 94 MHz), also implying the important role of THF in altering the ^{93}Nb EFG tensor. Using the approximated solid-state structure of **6**, with a Nb−Cp_{cen} distance of 2.06 Å, there is reasonable agreement between experimental and theoretical C_Q, but the values of η_Q are in disagreement. Theoretical calculations align V_{33} along the molecular axis; however, experimental parameters imply that V_{11} is the unique component, and that V_{22} and V_{33} are oriented in electronically similar environments, contrary to these predictions (Figure 12A). In light of the pseudo-octahedral structure of **7**, and previously reported dimeric structures of related compounds in the form $[\text{Cp}'\text{ZrLCl}_3]_2$,[115−119] it is possible that compound **6** forms a centro-symmetric bis-μ^2-chlorine-bridged dimer of the type depicted in Scheme 2, which may account for the discrepancy between experimental and theoretical parameters. However, we have not attempted to theoretically approximate the molecular structure of the dimer at this time, though future structural characterizations will focus on this problem.

Calculations on **7** were conducted upon molecular coordinates taken from both the major (61%) and minor (39%) occupancies used to refine the crystal structure. The value of C_Q is underestimated and overestimated by RHF and B3LYP calculations, respectively, though all calculations correctly predict C_Q to be larger than in the Nb(I) complexes and smaller than in compound **6**. The value of η_Q is predicted to have nearly axial symmetry in all cases except the RHF calculations on the structure with minor occupancy. The RHF and B3LYP calculations orient V_{33} very close to the direction of the Nb−O bond, with $\angle(V_{33}-\text{Nb}-\text{O})$ ca. 11° to 16° and 3° to 5°, respectively. V_{11} and V_{22} are in very similar electronic environments: for instance, in the B3LYP/6D calculations, both are directed toward the four Nb−Cl bonds (with dihedral angles, $\angle(V_{11/22}-\text{Nb}-\text{Cp}_{cen}-\text{Cl})$, ranging from 6° to 7°, Figure 12B). The crystal structure of **7** used for these calculations was obtained at −100 °C, so it might be expected that temperature-dependent structural changes are responsible for the divergence between experiment and theory. However, VT static ^{93}Nb NMR experiments on **7** reveal that there are relatively small changes in both the EFG and CS tensor parameters with changing temperature (Figure S5). As the temperature drops, C_Q decreases (Figure S6), which is different from the VT behavior in **1**. This distinct VT behavior in **7**, unlike in **1**, occurs because V_{33} is oriented near to the Nb−Cp_{cen} direction, and its magnitude is influenced by changes in Nb−Cp_{cen} distance.[36]

Niobium Chemical Shielding Tensors. There are several general observations that can be made after a review of the

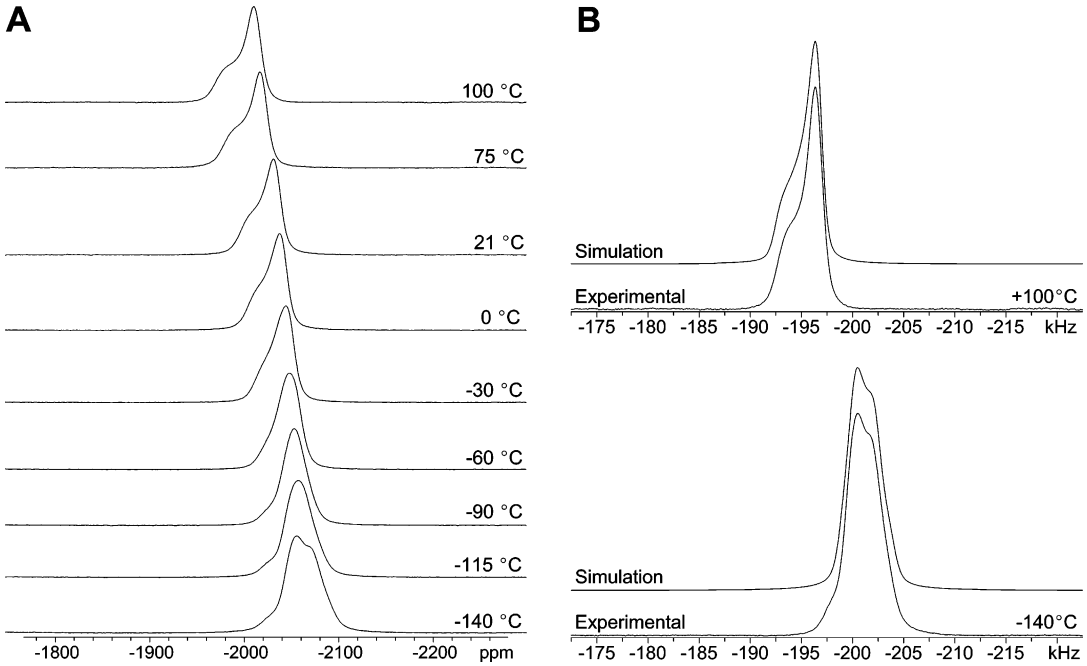

Figure 10. (A) VT ^{93}Nb static NMR spectra of **1** at 9.4 T. (B) Simulation reveals $C_Q = 2.0(10)$ MHz, $\eta_Q = 1.00(1)$, $\delta_{iso} = -2005.5(10)$ ppm, $\Omega = 43(2)$ ppm, $\kappa = -1.00(2)$, $\alpha = 70(10)°$, $\beta = 0(10)°$, and $\gamma = 20(20)°$ for +100 °C powder pattern in part A; and $C_Q = 5.0(2)$ MHz, $\eta_Q = 0.56(6)$, $\delta_{iso} = -2056.0(10)$ ppm, $\Omega = 34(2)$ ppm, $\kappa = -0.95(5)$, $\alpha = 90(20)°$, $\beta = 75(2)°$, and $\gamma = 45(45)°$ for −140 °C powder pattern in part A.

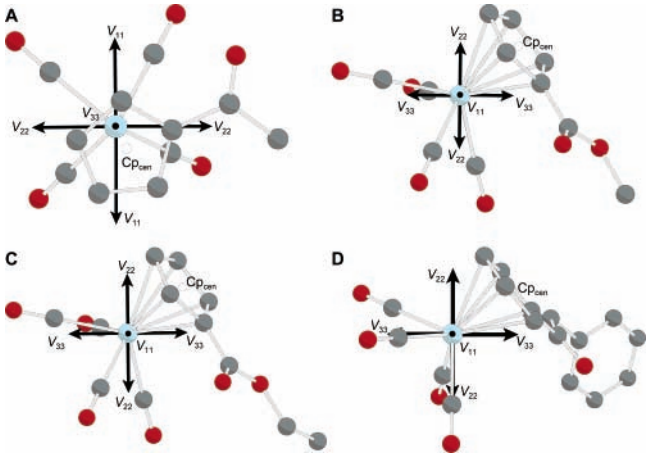

Figure 11. ^{93}Nb EFG tensor orientations for (A) **2**, (B) **3**, (C) **4**, and (D) **5**. Note that in part D, V_{22} is directed close to one of the Nb−CO bonds with $\angle(V_{22}-\text{Nb}-\text{CO}) \approx 20°$.

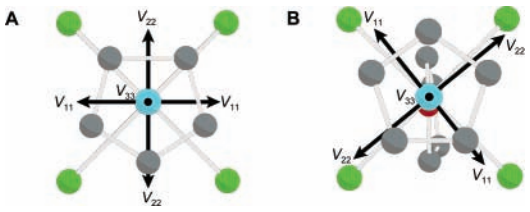

Figure 12. ^{93}Nb EFG tensor orientations for (A) **6** and (B) **7**.

niobium CS tensor data (Tables 6 and 7). Isotropic chemical shifts are not quantitatively predicted, though qualitative trends are observed. For instance, for a given set of calculations, Nb(I) complexes are predicted to have highly shielded ^{93}Nb nuclei in comparison to Nb(V) complexes. The lack of quantitative agreement between experiment and theory can be attributed to the overestimation of the spans of the niobium chemical shielding tensors. For **1**, calculations overestimate the experimentally measured span by an order of magnitude, perhaps

SCHEME 2: (A) Previously Reported Dimeric Structures of Compounds Related to 6 in the Form $[Cp'ZrLCl_3]_2$ and (B) Possible Structure of 6, Which Forms a Centrosymmetric Bis-μ^2-chlorine-Bridged Dimer

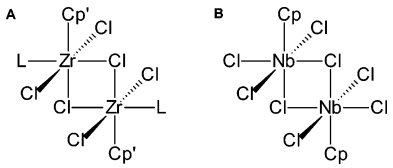

suggesting that motional averaging of the CS tensor is taking place (a similar observation was made for the ^{93}Nb EFG tensor above). For complexes **2** through **5**, RHF and B3LYP calculations consistently overestimate the spans, by about two times for the former and four times for the latter. RHF calculations predict the skews accurately for **1** and **2**, B3LYP calculations for **3** and **4**, while no calculation seems to predict the proper skew for **5**. For **6** and **7**, the spans are overestimated by a factor of ca. 3. The application of larger 6-311G(2d,p) and 6-311G(2df,p) basis sets, with and without diffuse functions, did not result in significant improvement (Supporting Information, Table S6). For instance, higher level calculations on **2** get closer to the experimentally predicted span, while incorrectly predicting the isotropic chemical shift. It is possible that the future use of relativistic DFT calculations incorporating the zeroth-order regular approximation (ZORA)[120−122] or the advent of superior Nb basis sets could improve quantitative agreement between experiment and theory.

All calculations predict similar CS tensor orientations, lending insight into the distinct magnetic shielding characteristics in Nb(I) and Nb(V) metallocenes. RHF calculations on the Nb(I) complexes predict that the most shielded component, δ_{33}, is oriented toward the Cp ring, with $\angle(\text{Cp}_{cen}-\text{Nb}-\delta_{33})$ angles ranging from 10° to 35°, whereas the B3LYP calculations consistently predict $\angle(\text{Cp}_{cen}-\text{Nb}-\delta_{33})$ angles even closer to zero. Both RHF and B3LYP calculations predict that the δ_{33} and V_{33} components are oriented in similar directions, with a

TABLE 5: Theoretical ^{93}Nb EFG Tensor Parameters in Nb(V) Complexes

source[a]	V_{11}[b] (au)	V_{22} (au)	V_{33} (au)	$\|C_Q\|$[c] (MHz)	η_Q
$CpNbCl_4$, **6**				**54.5(5)**[d]	**0.83(3)**
RHF/4F/6-311G**	0.2085	0.4721	−0.6806	51.2	0.39
RHF/6D/6-311G**	0.1937	0.4426	−0.6363	47.8	0.39
B3LYP/4F/6-311G**	0.338	0.5143	−0.8523	64.1	0.21
B3LYP/6D/6-311G**	0.301	0.4714	−0.7724	58.1	0.22
$CpNbCl_4$·THF, **7**				**38.4(4)**	**0.17(7)**
61% occ. RHF/4F/6-311G**[e]	0.1507	0.2257	−0.3764	28.3	0.2
61% occ. RHF/6D/6-311G**	0.1001	0.1816	−0.2817	21.2	0.29
61% occ. B3LYP/4F/6-311G**	0.3651	0.4372	−0.8023	60.3	0.09
61% occ. B3LYP/6D/6-311G**	0.297	0.36	−0.657	49.4	0.1
39% occ. RHF/4F/6-311G**	0.0916	0.2406	−0.3322	25	0.45
39% occ. RHF/6D/6-311G**	0.0394	0.1865	−0.226	17	0.65
39% occ. B3LYP/4F/6-311G**	0.3282	0.4461	−0.7743	58.2	0.15
39% occ. B3LYP/6D/6-311G**	0.2576	0.3656	−0.6232	46.9	0.17

[a] Source from theoretical work is in the form method/basis set (Nb)/basis set (all other atoms). [b] V_{ii} are the principal components of the ^{93}Nb EFG tensor such that $|V_{33}| \geq |V_{22}| \geq |V_{11}|$. [c] Absolute value of C_Q, where $C_Q = eQV_{33}/h$ and $\eta_Q = (V_{11} - V_{22})/V_{33}$. Theoretical C_Q are converted from atomic units to Hz (see Experimental Section for details). [d] Experimental values are provided in boldface for comparison. [e] Calculations were conducted upon molecular coordinates taken from both the major (61%) and minor (39%) occupancies used to refine the crystal structures.

TABLE 6: Theoretical Niobium CS Tensor Parameters in Nb(I) Complexes

source[a]	δ_{11}[b] (au)	δ_{22} (au)	δ_{33} (au)	δ_{iso}[c] (ppm)	Ω (ppm)	κ
$CpNb(CO)_4$, **1**	**−2004.3**[d]	**−2037.5**	**−2039.3**	**−2027(4)**	**35.0(5)**	**−0.90(5)**
RHF/4F/6-311G**	−1722.3	−1972.1	−1980.9	−1892	259	−0.93
RHF/6D/6-311G**	−1554	−1800	−1805.9	−1720	252	−0.95
B3LYP/4F/6-311G**	−2132.6	−2311.1	−2634.4	−2359	502	0.29
B3LYP/6D/6-311G**	−1949.3	−2120.1	−2428.8	−2166	479	0.29
$(MeOC)CpNb(CO)_4$, **2**	**−1859.5**	**−1922**	**−1984.5**	**−1922(2)**	**125(3)**	**0.00(2)**
RHF/4F/6-311G**	−1771	−1888.7	−2025.3	−1895	254	0.07
RHF/6D/6-311G**	−1615.9	−1716.5	−1838.3	−1724	222	0.1
B3LYP/4F/6-311G**	−2126.5	−2246	−2648.4	−2340	522	0.54
B3LYP/6D/6-311G**	−1951.1	−2058.4	−2437.8	−2149	487	0.56
$(MeO_2C)CpNb(CO)_4$, **3**	**−1858.8**	**−1919.5**	**−1993.8**	**−1924(4)**	**135(5)**	**0.10(5)**
RHF/4F/6-311G**	−1704.9	−1913.4	−1938.7	−1852	234	−0.78
RHF/6D/6-311G**	−1548.8	−1739	−1755.4	−1681	207	−0.84
B3LYP/4F/6-311G**	−2080.9	−2262.1	−2615.8	−2320	535	0.32
B3LYP/6D/6-311G**	−1905.3	−2071.9	−2405.7	−2128	500	0.33
$(EtO_2C)CpNb(CO)_4$, **4**	**−1864**	**−1912**	**−1984**	**−1920(1)**	**120(2)**	**0.20(4)**
RHF/4F/6-311G**	−1699.1	−1894.8	−1922.3	−1839	223	−0.75
RHF/6D/6-311G**	−1821.8	−2003.5	−2019.7	−1948	198	−0.84
B3LYP/4F/6-311G**	−2082.5	−2250.6	−2608.6	−2314	526	0.36
B3LYP/6D/6-311G**	−2168	−2326.6	−2663.5	−2386	495	0.36
$(PhH_2COC)CpNb(CO)_4$, **5**	**−1858.4**	**−1922.1**	**−1949.4**	**−1910(6)**	**91(4)**	**−0.40(20)**
RHF/4F/6-311G**	−1785.2	−1879.1	−1992.1	−1885	207	0.09
RHF/6D/6-311G**	−1625	−1714.3	−1805.6	−1715	181	0.01
B3LYP/4F/6-311G**	−2145.8	−2220.1	−2640.6	−2336	495	0.7
B3LYP/6D/6-311G**	−1967.8	−2038.1	−2428.7	−2145	461	0.69

[a] Source from theoretical work is in the form method/basis set (Nb)/basis set (all other atoms). [b] δ_{ii} are the principal components of the niobium CS tensor such that $\delta_{11} \geq \delta_{22} \geq \delta_{33}$. [c] Niobium CS tensor parameters: $\delta_{iso} = (\delta_{11} + \delta_{22} + \delta_{33})/3$, $\Omega = \delta_{11} - \delta_{33}$, and $\kappa = 3(\delta_{22} - \delta_{iso})/\Omega$. Niobium chemical shifts are referenced to 0.4 M $NbCl_5$ solution in CH_3CN (experimental) or $NbCl_6^-$ (theoretical), see Experimental Section for details. [d] Experimental values are provided in boldface for comparison.

notably reduced $\angle(V_{33}-Nb-\delta_{33})$ angle in the latter. Furthermore, in **1**, δ_{33} and δ_{11} are contained within the molecular mirror plane (Figure 13A), whereas in **2** through **5**, δ_{33} and δ_{22} are contained approximately in the pseudo-mirror planes of the molecule (i.e., planes that contain the first atom in the R groups, Figure 13B). In contrast, for the Nb(V) complexes, both RHF and B3LYP calculations predict that the least shielded component, δ_{11}, points toward the Cp ring. In **6**, δ_{11} is predicted to be oriented slightly away from the Cp ring centroid (Figure 13C), with $\angle(Cp_{cen}-Nb-\delta_{11})$ between 15° and 26°. However, in **7**, $\angle(Cp_{cen}-Nb-\delta_{11})$ is closer to 0° and $\angle(O-Nb-\delta_{11})$ is 3° to 5° (Figure 13D), suggesting that the presence of the THF ligand plays a major role in determining both the magnitude of the tensor components as well as their orientations in the molecular frame. Interestingly and uniquely in **7**, δ_{22} and δ_{33} point approximately toward the Nb−Cl bonds. Most calculations predict that $\angle(\delta_{33}-Nb-V_{33})$ are on the order of 90° (i.e., δ_{11} and V_{33} are relatively close to one another), in reasonable agreement with experimentally predicted tensor orientations.

A simplistic explanation for the large difference in chemical shifts between Nb(I) and Nb(V) complexes might be that since Nb(I) has more electron density than Nb(V), it should correspondingly be more shielded. However, the more accurate explanation is that chemical shielding tensor orientation and the magnitude of its components are altered as a result of differing interactions between Nb and the Cp ring, and Nb and the CO or Cl ligands. For Nb(I) complexes, δ_{33} is consistently oriented toward the Cp ring in the direction of the R group, while in the Nb(V) complexes, δ_{11} is oriented toward the Cp ring centroid. In $CpNbCl_4$·THF, there are occupied and virtual MOs which are close in energy and undergo symmetry-allowed magnetic-dipole mixing, oriented perpendicular to the $Nb-Cp_{cen}$ direction, resulting in deshielding parallel to the $Nb-Cp_{cen}$ direction. Such MOs are absent in the Nb(I) complexes, where CS tensor spans

TABLE 7: Theoretical Niobium CS Tensor Parameters in Nb(V) Complexes

source[a]	δ_{11}[b] (au)	δ_{22} (au)	δ_{33} (au)	δ_{iso}[c] (ppm)	Ω (ppm)	κ
$CpNbCl_4$, **6**	**−510.0**[d]	**−630**	**−660**	**−600(30)**	**150(30)**	**−0.60(4)**
RHF/4F/6-311G**	−356.6	−474.3	−791.3	−541	435	0.46
RHF/6D/6-311G**	−254.5	−468.6	−738.3	−487	484	0.11
B3LYP/4F/6-311G**	−121.8	−507.4	−581.5	−404	460	−0.68
B3LYP/6D/6-311G**	−97.9	−498.8	−566	−388	468	−0.71
$CpNbCl_4$·THF, **7**	**−521.7**	**−745.7**	**−841.7**	**−703(12)**	**320(10)**	**−0.40(20)**
61% occ. RHF/4F/6-311G**[e]	−582.9	−1305	−1402	−1097	819	−0.76
61% occ. RHF/6D/6-311G**	−434.5	−1205	−1301	−980	866	−0.78
61% occ. B3LYP/4F/6-311G**	−239.1	−1193	−1254	−895	1015	−0.88
61% occ. B3LYP/6D/6-311G**	−167	−1119	−1180	−822	1012	−0.88
39% occ. RHF/4F/6-311G**	−596.7	−1328	−1429	−1118	832	−0.76
39% occ. RHF/6D/6-311G**	−446	−1230	−1326	−1001	880	−0.78
39% occ. B3LYP/4F/6-311G**	−241.9	−1196	−1285	−907	1043	−0.83
39% occ. B3LYP/6D/6-311G**	−168.7	−1123	−1209	−834	1040	−0.83

[a] Source from theoretical work is in the form method/basis set (Nb)/basis set (all other atoms). [b] δ_{ii} are the principal components of the niobium CS tensor such that $\delta_{11} \geq \delta_{22} \geq \delta_{33}$. [c] Niobium CS tensor parameters: $\delta_{iso} = (\delta_{11} + \delta_{22} + \delta_{33})/3$, $\Omega = \delta_{11} - \delta_{33}$, and $\kappa = 3(\delta_{22} - \delta_{iso})/\Omega$. Niobium chemical shifts are referenced to 0.4 M $NbCl_5$ solution in CH_3CN (experimental) or $NbCl_6^-$ (theoretical), see Experimental Section for details. [d] Experimental values are provided in boldface for comparison. [e] Calculations were conducted upon molecular coordinates taken from both the major (61%) and minor (39%) occupancies used to refine the crystal structure.

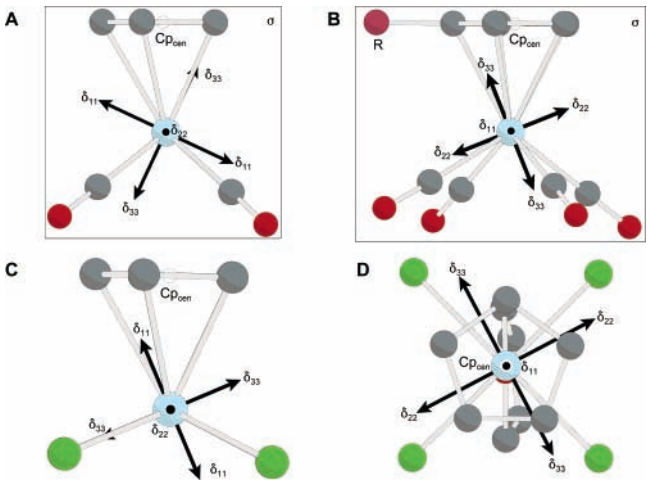

Figure 13. Niobium CS tensor orientations for (A) **1**, (B) **2** through **5**, (C) **6**, and (D) **7**.

are much smaller, accounting for the large difference in shielding parameters. Thus, though the exact CS tensor orientations are not duplicated in all calculations, there is still the overall inference that very different chemical shielding mechanisms are at work in the Nb(I) and Nb(V) complexes. Future detailed MO analyses will provide further insight into the magnetic shielding of transition metals in this important class of compounds.

Conclusions

Solid-state ^{93}Nb NMR spectroscopy, complemented by ^{13}C NMR experiments, has been shown to be a very sensitive and rapid probe of molecular structure and purity in half-sandwich metallocenes. Static, MAS, and piecewise ^{93}Nb QCPMG NMR experiments can be conducted with relative ease, and provide spectra which are rich in information on structure and dynamics. Subtle functional group changes on the Cp′ ring result in observable changes in the ^{93}Nb quadrupolar and chemical shift parameters. An immense increase in the quadrupolar interaction is witnessed upon changing the nature of the other coordinating ligands (CO to Cl) and formal oxidation state of the Nb atom (I to V). The increased quadrupolar interaction in $CpNbCl_4$ results in a pattern whose breadth exceeds uniform excitation bandwidths using 1 kW amplifiers and standard magnetic field strengths; notwithstanding, piecewise QCPMG experiments can be applied to rapidly acquire a powder pattern from which relevant NMR tensor parameters can be extracted. Attempts to grow a single crystal of pure $CpNbCl_4$ have resulted in the isolation of a new solvent-coordinated species, $CpNbCl_4$·THF, which has been characterized by both solid-state NMR and X-ray crystallographic methods. The presence of THF results in a dramatic alteration of the ^{93}Nb quadrupolar interaction and spectral appearance, so much so, that it can be acquired within a single experiment, contrary to its unligated parent complex. Preliminary theoretical calculations of NMR tensor parameters do not display high levels of precision in terms of quantitative agreement with experiment, in a few cases due to the approximate nature of the available models used for calculations. Qualitative trends, however, in both quadrupolar and chemical shielding parameters are well reproduced, and most importantly, EFG and CS tensor orientations lend insight into the origins of NMR interactions and their relationships to molecular structure, symmetry, and dynamics. This comprehensive study of niobium metallocenes suggests that complimentary data derived from solid-state ^{93}Nb and ^{13}C NMR experiments, X-ray diffraction techniques, and first principles calculations will be very useful in characterizing organometallic niobium species in a variety of crystalline and disordered solid materials of fundamental, technological, and/or industrial importance.

Acknowledgment. This research was funded by Imperial Oil and the Natural Sciences and Engineering Research Council (NSERC−Canada). R.W.S. thanks the Canadian Foundation for Innovation (CFI), the Ontario Innovation Trust (OIT), and the University of Windsor for funding the Solid-State NMR facility at the University of Windsor. The Centre for Catalysis and Materials Research (CCMR) at the University is thanked for additional funding. We thank Mr. Michael Fuerth for his assistance with experiments on the Bruker 500 MHz instrument. We also thank Professor Samuel A. Johnson at the University of Windsor for his assistance with the sublimation experiment.

Supporting Information Available: Tables of crystallographic data, structural parameters used in theoretical calculations, NMR tensor parameters from theoretical calculations, and additional ^{93}Nb and ^{13}C NMR spectra as well as a CIF file. This material is available free of charge via the Internet at http://pubs.acs.org.

References and Notes

(1) Wilkinson, G.; Rosenblum, M.; Whiting, M. C.; Woodward, R. B. *J. Am. Chem. Soc.* **1952**, *74*, 2125.

(2) Bochmann, M. *Organometallics 2, Complexes with Transition Metal−Carbon B-Bonds*; Oxford University Press Inc.: New York, 1994.

(3) Togni, A.; Halterman, R. L. *Metallocenes−Synthesis, Reactivity, Applications*; Wiley-VCH: New York, 1998; Vol. 2.

(4) Klipp, A.; Hamelmann, F.; Haindl, G.; Hartwich, J.; Kleineberg, U.; Jutzi, P.; Heinzmann, U. *Chem. Vap. Deposition* **2000**, *6*, 63.

(5) Beswick, M. A.; Palmer, J. S.; Wright, D. S. *Chem. Soc. Rev.* **1998**, *27*, 225.

(6) Klipp, A.; Petri, S. H. A.; Neumann, B.; Stammler, H. G.; Jutzi, P. *J. Organomet. Chem.* **2001**, *620*, 20.

(7) Mashima, K.; Fujikawa, S.; Tanaka, Y.; Urata, H.; Oshiki, T.; Tanaka, E.; Nakamura, A. *Organometallics* **1995**, *14*, 2633.

(8) Antinolo, A.; Carrillo-Hermosilla, F.; Fajardo, M.; Fernandez-Baeza, J.; Garcia-Yuste, S.; Otero, A. *Coord. Chem. Rev.* **1999**, *195*, 43.

(9) Imanishi, Y.; Naga, N. *Prog. Polym. Sci.* **2001**, *26*, 1147.

(10) Bitterwolf, T. E.; Gallagher, S.; Bays, J. T.; Scallorn, B.; Rheingold, A. L.; Guzei, I. A.; Liable-Sands, L.; Linehan, J. C. *J. Organomet. Chem.* **1998**, *557*, 77.

(11) Herrmann, W. A.; Kalcher, W.; Biersack, H.; Bernal, I.; Creswick, M. *Chem. Ber.-Recl.* **1981**, *114*, 3558.

(12) Tenhaeff, S. C.; Tyler, D. R. *Organometallics* **1991**, *10*, 1116.

(13) Tenhaeff, S. C.; Tyler, D. R. *Organometallics* **1991**, *10*, 473.

(14) Bechthold, H. C.; Rehder, D. *J. Organomet. Chem.* **1981**, *206*, 305.

(15) Bitterwolf, T. E.; Gallagher, S.; Rheingold, A. L.; Yap, G. P. A. *J. Organomet. Chem.* **1997**, *546*, 27.

(16) Herrmann, W. A.; Biersack, H.; Ziegler, M. L.; Weidenhammer, K.; Siegel, R.; Rehder, D. *J. Am. Chem. Soc.* **1981**, *103*, 1692.

(17) Lichtenberger, D. L.; Fan, H. J.; Gruhn, N. E.; Bitterwolf, T. E.; Gallagher, S. *Organometallics* **2000**, *19*, 2012.

(18) Earp, J. C.; Margolis, D. S.; Tanjaroon, C.; Bitterwolf, T. E.; Kukolich, S. G. *J. Mol. Spectrosc.* **2002**, *211*, 82.

(19) Naumann, F.; Rehder, D.; Pank, V. *J. Organomet. Chem.* **1982**, *240*, 363.

(20) Gibson, V. C.; Williams, D. N.; Clegg, W.; Hockless, D. C. R. *Polyhedron* **1989**, *8*, 1819.

(21) Williams, D. N.; Mitchell, J. P.; Poole, A. D.; Siemeling, U.; Clegg, W.; Hockless, D. C. R.; Oneil, P. A.; Gibson, V. C. *J. Chem. Soc., Dalton Trans.* **1992**, 739.

(22) Fettinger, J. C.; Keogh, D. W.; Poli, R. *Inorg. Chem.* **1995**, *34*, 2343.

(23) Blaurock, S.; Hey-Hawkins, E. *Z. Anorg. Allg. Chem.* **2002**, *628*, 2515.

(24) Rehder, D.; Paulsen, K.; Basler, W. *J. Magn. Reson.* **1983**, *53*, 500.

(25) Gobetto, R.; Harris, R. K.; Apperley, D. C. *J. Magn. Reson.* **1992**, *96*, 119.

(26) Gibson, V. C.; Gobetto, R.; Harris, R. K.; Langdalebrown, C.; Siemeling, U. *J. Organomet. Chem.* **1994**, *479*, 207.

(27) Hallock, K. J.; Lee, D. K.; Ramamoorthy, A. *Chem. Phys. Lett.* **1999**, *302*, 175.

(28) Sporer, C.; Heise, H.; Wurst, K.; Ruiz-Molina, D.; Kopacka, H.; Jaitner, P.; Kohler, F.; Novoa, J. J.; Veciana, J. *Chem.-Eur. J.* **2004**, *10*, 1355.

(29) He, X.; Lo, A. Y. H.; Trudeau, M.; Schurko, R. W.; Antonelli, D. *Inorg. Chem.* **2003**, *42*, 335.

(30) Honnerscheid, A.; van Wullen, L.; Jansen, M.; Rahmer, J.; Mehring, M. *J. Chem. Phys.* **2001**, *115*, 7161.

(31) Heise, H.; Kohler, F. H.; Xie, X. L. *J. Magn. Reson.* **2001**, *150*, 198.

(32) Endregard, M.; Nicholson, D. G.; Stocker, M.; Lamble, G. M. *J. Mater. Chem.* **1995**, *5*, 785.

(33) Uusitalo, A. M.; Pakkanen, T. T.; Iskola, E. I. *J. Mol. Catal. A: Chem.* **2002**, *177*, 179.

(34) Schnellbach, M.; Kohler, F. H.; Blumel, J. *J. Organomet. Chem.* **1996**, *520*, 227.

(35) Schurko, R. W.; Hung, I.; Schauff, S.; Macdonald, C. L. B.; Cowley, A. H. *J. Phys. Chem. A* **2002**, *106*, 10096.

(36) Willans, M. J.; Schurko, R. W. *J. Phys. Chem. B* **2003**, *107*, 5144.

(37) Edwards, A. J.; Burke, N. J.; Dobson, C. M.; Prout, K.; Heyes, S. J. *J. Am. Chem. Soc.* **1995**, *117*, 4637.

(38) Schurko, R. W.; Hung, I.; Macdonald, C. L. B.; Cowley, A. H. *J. Am. Chem. Soc.* **2002**, *124*, 13204.

(39) Iiskola, E. I.; Timonen, S.; Pakkanen, T. T.; Harkki, O.; Lehmus, P.; Seppala, J. V. *Macromolecules* **1997**, *30*, 2853.

(40) Hung, I.; Schurko, R. W. *Solid State Nucl. Magn. Reson.* **2003**, *24*, 78.

(41) Hung, I.; Macdonald, C. L. B.; Schurko, R. W. *Chem.-Eur. J.* **2004**, *10*, 5923.

(42) Hung, I.; Schurko, R. W. *J. Phys. Chem. B* **2004**, *108*, 9060.

(43) Johnels, D.; Boman, A.; Edlund, U. *Magn. Reson. Chem.* **1998**, *36*, S151.

(44) Pietrass, T.; Burkert, P. K. *Inorg. Chim. Acta* **1993**, *207*, 253.

(45) Pietrass, T.; Burkert, P. K. *Z. Naturforsch., B: Chem. Sci.* **1993**, *48*, 1555.

(46) Janiak, C.; Schumann, H.; Stader, C.; Wrackmeyer, B.; Zuckerman, J. J. *Chem. Ber.-Recl.* **1988**, *121*, 1745.

(47) Wrackmeyer, B.; Kupce, E.; Kehr, G.; Sebald, A. *Magn. Reson. Chem.* **1992**, *30*, 964.

(48) Armstrong, D. R.; Duer, M. J.; Davidson, M. G.; Moncrieff, D.; Russell, C. A.; Stourton, C.; Steiner, A.; Stalke, D.; Wright, D. S. *Organometallics* **1997**, *16*, 3340.

(49) Keates, J. M.; Lawless, G. A. *Organometallics* **1997**, *16*, 2842.

(50) Spiess, H. W.; Haas, H.; Hartmann, H. *J. Chem. Phys.* **1969**, *50*, 3057.

(51) Pyykko, P. *Mol. Phys.* **2001**, *99*, 1617.

(52) Gabuda, S. P.; Zil'berman, B. D.; Goncharuk, V. K. *Zh. Strukt. Khim.* **1978**, 431.

(53) Ponce, A. L.; Lin, X.; Fripiat, J. J. *Solid State Ionics* **1996**, *84*, 213.

(54) Creel, R. B.; Segel, S. L.; Schoenberger, R. J.; Barnes, R. G.; Torgeson, D. R. *J. Chem. Phys.* **1974**, *60*, 2310.

(55) Barnes, R. G.; Roenker, K. P.; Brooker, H. R. *Ber. Bunsen-Ges. Phys. Chem. Chem. Phys.* **1976**, *80*, 875.

(56) Du, L. S.; Schurko, R. W.; Kim, N.; Grey, C. P. *J. Phys. Chem. A* **2002**, *106*, 7876.

(57) Du, L. S.; Schurko, R. W.; Lim, K. H.; Grey, C. P. *J. Phys. Chem. A* **2001**, *105*, 760.

(58) Ivanova, E. N.; Yatsenko, A. V.; Sergeev, N. A. *Solid State Nucl. Magn. Reson.* **1995**, *4*, 381.

(59) Blumel, J.; Born, E.; Metzger, T. *J. Phys. Chem. Solids* **1994**, *55*, 589.

(60) Bastow, T. J. *Z. Naturforsch., A: Phys. Sci.* **1994**, *49*, 320.

(61) Geselbracht, M. J.; Stacy, A. M.; Garcia, A. R.; Silbernagel, B. G.; Kwei, G. H. *J. Phys. Chem.* **1993**, *97*, 7102.

(62) Peterson, G. E.; Bridenbaugh, P. M. *J. Chem. Phys.* **1968**, *48*, 3402.

(63) Kind, R.; Graenicher, H.; Derighetti, B.; Waldner, F.; Brun, E. *Solid State Commun.* **1968**, *6*, 439.

(64) Douglass, D. C.; Peterson, G. E.; McBrierty, V. J. *Phys. Rev. B* **1989**, *40*, 10694.

(65) Norcross, J. A.; Ailion, D. C.; Blinc, R.; Dolinsek, J.; Apih, T.; Slak, J. *Phys. Rev. B* **1994**, *50*, 3625.

(66) Meadows, M. D.; Smith, K. A.; Kinsey, R. A.; Rothgeb, T. M.; Skarjune, R. P.; Oldfield, E. *Proc. Natl. Acad. Sci. U.S.A.* **1982**, *79*, 1351.

(67) Cruz, L. P.; Savariault, J. M.; Rocha, J.; Jumas, J. C.; Pedrosa de Jesus, J. D. *J. Solid State Chem.* **2001**, *156*, 349.

(68) Fitzgerald, J. J.; Prasad, S.; Huang, J.; Shore, J. S. *J. Am. Chem. Soc.* **2000**, *122*, 2556.

(69) Avogadro, A.; Bonera, G.; Borsa, F.; Rigamonti, A. *Phys. Rev. B* **1974**, *9*, 3905.

(70) Wolf, F.; Kline, D.; Story, H. S. *J. Chem. Phys.* **1970**, *53*, 3538.

(71) Man, P. P.; Theveneau, H.; Papon, P. *J. Magn. Reson.* **1985**, *64*, 271.

(72) Ashbrook, S. E.; Wimperis, S. *J. Magn. Reson.* **2002**, *156*, 269.

(73) Prasad, S.; Zhao, P.; Huang, J.; Fitzgerald, J. J.; Shore, J. S. *Solid State Nucl. Magn. Reson.* **1999**, *14*, 231.

(74) Prasad, S.; Zhao, P.; Huang, J.; Fitzgerald, J. J.; Shore, J. S. *Solid State Nucl. Magn. Reson.* **2001**, *19*, 45.

(75) Muntean, L.; Ailion, D. C. *Phys. Rev. B* **2001**, *6301*.

(76) Zhou, D. H.; Hoatson, G. L.; Vold, R. L. *J. Magn. Reson.* **2004**, *167*, 242.

(77) Larsen, F. H.; Jakobsen, H. J.; Ellis, P. D.; Nielsen, N. C. *J. Phys. Chem. A* **1997**, *101*, 8597.

(78) Larsen, F. H.; Nielsen, N. C. *J. Phys. Chem. A* **1999**, *103*, 10825.

(79) Pangborn, A. B.; Giardello, M. A.; Grubbs, R. H.; Rosen, R. K.; Timmers, F. J. *Organometallics* **1996**, *15*, 1518.

(80) Jager, C.; Mullerwarmuth, W.; Mundus, C.; Vanwullen, L. *J. Non-Cryst. Solids* **1992**, *149*, 209.

(81) Eichele, K.; Wasylishen, R. E. *WSOLIDS*, v. 1.17.30 ed.; Tübingen, 2001.

(82) Bak, M.; Rasmussen, J. T.; Nielsen, N. C. *J. Magn. Reson.* **2000**, *147*, 296.

(83) Frisch, M. J.; Trucks, G. W.; Schlegel, H. B.; Scuseria, G. E.; Robb, M. A.; Cheeseman, J. R.; Zakrzewski, V. G.; Montgomery, J. A., Jr.; Stratmann, R. E.; Burant, J. C.; Dapprich, S.; Millam, J. M.; Daniels, A. D.; Kudin, K. N.; Strain, M. C.; Farkas, O.; Tomasi, J.; Barone, V.; Cossi, M.; Cammi, R.; Mennucci, B.; Pomelli, C.; Adamo, C.; Clifford, S.; Ochterski, J.; Petersson, G. A.; Ayala, P. Y.; Cui, Q.; Morokuma, K.; Malick, D. K.; Rabuck, A. D.; Raghavachari, K.; Foresman, J. B.; Cioslowski, J.; Ortiz, J. V.; Baboul, A. G.; Stefanov, B. B.; Liu, G.; Liashenko, A.; Piskorz, P.; Komaromi, I.; Gomperts, R.; Martin, R. L.; Fox, D. J.; Keith, T.; Al-Laham, M. A.; Peng, C. Y.; Nanayakkara, A.; Challacombe, M.; Gill, P. M. W.; Johnson, B.; Chen, W.; Wong, M. W.; Andres, J. L.; Gonzalez, C.;

Head-Gordon, M.; Replogle, E. S.; Pople, J. A. *Gaussian 98*, Revision A.9; Gaussian, Inc.: Pittsburgh, PA, 1998.

(84) Frisch, M. J.; Trucks, G. W.; Schlegel, H. B.; Scuseria, G. E.; Robb, M. A.; Cheeseman, J. R.; Montgomery, J. A., Jr.; Vreven, T.; Kudin, K. N.; Burant, J. C.; Millam, J. M.; Iyengar, S. S.; Tomasi, J.; Barone, V.; Mennucci, B.; Cossi, M.; Scalmani, G.; Rega, N.; Petersson, G. A.; Nakatsuji, H.; Hada, M.; Ehara, M.; Toyota, K.; Fukuda, R.; Hasegawa, J.; Ishida, M.; Nakajima, T.; Honda, Y.; Kitao, O.; Nakai, H.; Klene, M.; Li, X.; Knox, J. E.; Hratchian, H. P.; Cross, J. B.; Adamo, C.; Jaramillo, J.; Gomperts, R.; Stratmann, R. E.; Yazyev, O.; Austin, A. J.; Cammi, R.; Pomelli, C.; Ochterski, J. W.; Ayala, P. Y.; Morokuma, K.; Voth, G. A.; Salvador, P.; Dannenberg, J. J.; Zakrzewski, V. G.; Dapprich, S.; Daniels, A. D.; Strain, M. C.; Farkas, O.; Malick, D. K.; Rabuck, A. D.; Raghavachari, K.; Foresman, J. B.; Ortiz, J. V.; Cui, Q.; Baboul, A. G.; Clifford, S.; Cioslowski, J.; Stefanov, B. B.; Liu, G.; Liashenko, A.; Piskorz, P.; Komaromi, I.; Martin, R. L.; Fox, D. J.; Keith, T.; Al-Laham, M. A.; Peng, C. Y.; Nanayakkara, A.; Challacombe, M.; Gill, P. M. W.; Johnson, B.; Chen, H.; Wong, M. W.; Gonzalez, C.; Pople, J. A. *Gaussian 03*, Rev. B.03; Gaussian, Inc.: Pittsburgh, PA, 2003.

(85) Huzinaga S., A. J. *Gaussian basis sets for molecular calculations*; Elsevier: New York, 1984.

(86) Coriani, S.; Hattig, C.; Jorgensen, P.; Rizzo, A.; Ruud, K. *J. Chem. Phys.* **1998**, *109*, 7176.

(87) Ditchfield, R. *Mol. Phys.* **1974**, *27*, 789.

(88) Wolinski, K.; Hinton, J. F.; Pulay, P. *J. Am. Chem. Soc.* **1990**, *112*, 8251.

(89) Shelyapina, M. G.; Kasperovich, V. S.; Shchegolev, B. F.; Charnaya, E. V. *Phys. Status Solidi B* **2001**, *225*, 171.

(90) Altomare, A.; Burla, M. C.; Camalli, M.; Cascarano, G.; Giacovazzo, C.; Guagliardi, A.; G., M. A. G.; Polidori, G.; Spagna, R. *SIR97*; CNR-IRMEC: Bari, 1997.

(91) Sheldrick, G. M. *SHELXL-97*; Universitat Gottingen: Gottingen, 1997.

(92) Wilson, A. J. C., Ed. *International Tables for X-ray Crystallography*; Kluwer Academic Press: Boston, MA, 1992; Vol. C.

(93) Sheldrick, G. M. *SHELXTL*; Bruker AXS Inc.: Madison, WI, 2001.

(94) Kraus, W.; Nolze, G. *PowderCell*, v. 2.4; Federal Institute for Materials Research and Testing: Berlin, Germany, 2000.

(95) Power, W. P.; Wasylishen, R. E.; Mooibroek, S.; Pettitt, B. A.; Danchura, W. *J. Phys. Chem.* **1990**, *94*, 591.

(96) Mason, J., Ed. *Multinuclear NMR*; Plenum Publishing Corporation: New York, 1987.

(97) Schreckenbach, G. *J. Chem. Phys.* **1999**, *110*, 11936.

(98) Rehder, D.; Bechthold, H. C.; Kececi, A.; Schmidt, H.; Siewing, M. *Z. Naturforsch., B*: *Chem. Sci.* **1982**, *37*, 631.

(99) Pforr, I.; Naeumann, F.; Rehder, D. *J. Organomet. Chem.* **1983**, *258*, 189.

(100) Hoch, M.; Rehder, D. *Z. Naturforsch. B* **1983**, *38B*, 446.

(101) Schmidt-Rohr, K.; Spiess, H. W. *Multidimensional Solid-State NMR and Polymers*; Academic Press: Toronto, Canada, 1994.

(102) Massiot, D.; Farnan, I.; Gautier, N.; Trumeau, D.; Trokiner, A.; Coutures, J. P. *Solid State Nucl. Magn. Reson.* **1995**, *4*, 241.

(103) Medek, A.; Frydman, V.; Frydman, L. *J. Phys. Chem. A* **1999**, *103*, 4830.

(104) Lipton, A. S.; Wright, T. A.; Bowman, M. K.; Reger, D. L.; Ellis, P. D. *J. Am. Chem. Soc.* **2002**, *124*, 5850.

(105) Alcalde, M. I.; Delamata, J.; Gomez, M.; Royo, P.; Pellinghelli, M. A.; Tiripicchio, A. *Organometallics* **1994**, *13*, 462.

(106) Herzfeld, J.; Berger, A. E. *J. Chem. Phys.* **1980**, *73*, 6021.

(107) Sayer, I. *J. Chem. Soc., Chem. Commun.* **1988**, 227.

(108) Kentgens, A. P. M.; Karrenbeld, H.; Deboer, E.; Schumann, H. *J. Organomet. Chem.* **1992**, *429*, 99.

(109) Orendt, A. M.; Facelli, J. C.; Jiang, Y. J.; Grant, D. M. *J. Phys. Chem. A* **1998**, *102*, 7692.

(110) Gay, I. D.; Young, G. B. *Organometallics* **1996**, *15*, 2264.

(111) Crosby, R. C.; Haw, J. F.; Lewis, D. H. *Anal. Chem.* **1988**, *60*, 2695.

(112) Harris, R. K.; Olivieri, A. C. *Prog. Nucl. Magn. Reson. Spectrosc.* **1992**, *24*, 435.

(113) Wasylishen, R. E.; Wright, K. C.; Eichele, K.; Cameron, T. S. *Inorg. Chem.* **1994**, *33*, 407.

(114) Kao, H. M.; Lii, K. H. *Inorg. Chem.* **2002**, *41*, 5644.

(115) Enders, M.; Rudolph, R.; Pritzkow, H. *Chem. Ber.* **1996**, *129*, 459.

(116) Krutko, D. P.; Borzov, M. V.; Petrosyan, V. S.; Kuzmina, L. G.; Churakov, A. V. *Russ. Chem. Bull.* **1996**, *45*, 1740.

(117) Krutko, D. P.; Borzov, M. V.; Petrosyan, V. S.; Kuzmina, L. G.; Churakov, A. V. *Russ. Chem. Bull.* **1996**, *45*, 940.

(118) Lancaster, S. J.; Thornton-Pett, M.; Dawson, D. M.; Bochmann, M. *Organometallics* **1998**, *17*, 3829.

(119) vanderZeijden, A. A. H.; Mattheis, C.; Frohlich, R. *Organometallics* **1997**, *16*, 2651.

(120) Wolff, S. K.; Ziegler, T.; van Lenthe, E.; Baerends, E. J. *J. Chem. Phys.* **1999**, *110*, 7689.

(121) Bouten, R.; Baerends, E. J.; van Lenthe, E.; Visscher, L.; Schreckenbach, G.; Ziegler, T. *J. Phys. Chem. A* **2000**, *104*, 5600.

(122) Ooms, K. J.; Wasylishen, R. E. *J. Am. Chem. Soc.* **2004**, *126*, 10972.